Ultraphytoplankton community structure in subsurface waters along a North-South Mediterranean transect

Ismail Boudriga, Melilotus Thyssen, Amel Zouari, Nicole Garcia, Marc Tedetti, Malika Bel Hassen

Ultraphytoplankton community structure in subsurface waters along a North-South Mediterranean transect

Ismail Boudriga[a], Melilotus Thyssen[b], Amel Zouari[a], Nicole Garcia[b], Marc Tedetti[b], Malika Bel Hassen[a]

[a] Institut National des Sciences et Technologies de la Mer (INSTM); 28, rue 2 mars 1934, Salammbô 2025, Tunisia
[b] Aix Marseille Univ., Université de Toulon, CNRS, IRD, MIO UM 110, 13288, Marseille, France

* Corresponding author: med.ismail.boudriga@gmail.com

Abstract

The subsurface ultraphytoplanktonic (< 10 µm) community was assessed along a North-South round-trip Mediterranean transect in the framework of the MERITE-HIPPOCAMPE cruise held on April - May 2019. Along the transect, various additional variables were measured in subsurface waters (2-5 m depth): temperature, salinity, and nutrient concentrations. The subsurface ultraphytoplankton community structure was resolved with a few kilometers' spatial resolution and 30-min temporal resolution using an automated pulse shape recording flow cytometer. The subsurface waters were clustered into seven areas based on their temperature and salinity characteristics. *Synechococcus* were by far the most abundant in all prospected zones and nanoeukaryotes were the main biomass contributors representing up to 51% of the ultraphytoplankton carbon biomass. A decreasing gradient in the apparent net primary productivity (NPP) was observed along the transect from north to south, with an NPP mostly sustained by *Synechococcus* in all zones. The results could have several implications in the trophic transfer of contaminants in planktonic food webs as it highlights the potential role of nanoplankton in bioaccumulation processes and that of *Synechococcus* in a likely transfer *via* grazing activities.

1. Introduction

Phytoplankton, which represents only 0.2% of the global autotrophic biomass, is responsible for roughly 50% of the net primary production on earth (i.e., 50 Pg C $year^{-1}$) (Falkowski et al., 1998; Field et al., 1998; Chavez et al., 2011). To understand the exact role of phytoplankton in the biogeochemical cycles, biological carbon pump (Siegenthaler and Sarmiento, 1993), and transfer of energy and matter within the trophic web (Sakka-Hlailli et al., 2014), its characterization in terms of size spectrum, communities/species and their relative production is essential at appropriate spatiotemporal frame.

Mapping the dynamic distribution of phytoplankton is affected by the sampling and measuring methods used. As an example, the fractional contribution of phytoplankton populations to bulk biomass can be measured from remote sensing using signature of diagnostic pigments (Ciotti and Bricaud, 2006; Brewin et al., 2010; Hirata et al., 2011), but these large-scale observations suffer from small spatio-temporal scale resolution (Levy et al.,2003). Single-cell analyses permitted by flow cytometry combined with in situ and automated sampling can observe fine-scale temporal dynamics of phytoplankton (Dubelaar and Gerritzen, 2000; Thyssen et al., 2008, 2014). Moreover, the most efficient method for quantifying phytoplankton productivity is the estimation of the dividing rate of a population in relation to the cell cycle. The use of several optical properties, based on periodic increase and decrease in light scatter intensity, interpreted as a response of cellular growth and division occurring during the cell cycle (Durand 1995; Binder et al., 1996), linked to cell size gives a good growth rates estimation. Diel variations in the phytoplankton cell dimensions was used as an automated measurement to calculate growth rates of natural phytoplanktonic groups during flow cytometry high frequency surveys (Sosik et al., 2003). This approach has been used to investigate the variability of primary production in different trophic conditions such as in eutrophic bloom areas (Campbell et al., 2010; Brosnahan et al., 2015) to oligotrophic ecosystems (Hunter-Cervera et al., 2014; Ribalet et al., 2015).

In the Mediterranean Sea, pigment analysis revealed that more than 80% of the autotrophic biomass originated from the nanoplanktonic and picoplanktonic sized groups (Vidussi et al., 2001; Bel Hassen et al., 2009). These size fractions seem to play a crucial role in the energy transfer to higher trophic levels mainly in oligotrophic marine areas such as the Mediterranean Sea (Pulido-Villena et al., 2014). Moreover, the lower trophic levels of pelagic ecosystems, such as phytoplankton and heterotrophic prokaryotes, are particularly exposed to various metallic and organic contaminants for which the bioconcentration is governed by sorption between the surrounding water and the cells (Wallberg et al., 1997; Sobek and Gustafsson, 2004; Nizzetto et al., 2012). Therefore, characterizing these populations in terms of functional diversity, contribution to bulk fluorescence, carbon biomass and growth rate will provide valuable information on their role in the energy transfer but also in the potential accumulation and transfer of contaminants within planktonic food web, which are strongly influenced by the species/size structure and biomass of plankton community (Alekseenko et al., 2018; Chouvelon et al., 2019).

The present study investigates the subsurface ultraphytoplankton distribution along a North-South transect in the Mediterranean Sea using high frequency pulse shape recording flow cytometry in the framework of the MERITE-HIPPOCAMPE cruise. This cruise aimed at studying the accumulation and transfer of metallic and organic contaminants at the atmosphere/water/plankton interfaces and within the plankton food webs (phyto-, zoo- and bacterio-plankton) in areas of scientific and economic interests of the Mediterranean Sea. The main objectives of the present paper are: 1) To characterize the ultraphytoplankton community structure in terms of abundance, biomass, red fluorescence, and apparent growth rate along the North-South Mediterranean transect that crosses areas with different physical structures, hydrological and biogeochemical conditions, and anthropogenic pressures. 2) To assess the productivity of each resolved group in order to provide clues on the phytoplanktonic population turnover and their potential implications in the carbon cycle, and eventually the transfer of contaminants within the plankton food webs.

2. Material and Methods

2.1. Stations and sampling

The MERITE-HIPPOCAMPE cruise was carried out in spring, from 13 April and 14 May 2019, on board the R/V *Antéa*, along a North-South round trip transect from the French coast (La Seyne-sur-mer; North-western Mediterranean Sea) to the Gulf of Gabès in Tunisia (South-eastern Mediterranean Sea) (Tedetti and Tronczynski, 2019) (Fig. 1). The investigation period was divided into two sub-periods Leg 1 and Leg 2. Leg1, from 13 to 28 April, was dedicated to the southward transect, between La Seyne-sur-mer and Tunis, with sampling of five long stations: St2, St4, St3, St10 and St11. Leg2, from 30 April to 14 May, covered the end of the transect to the south (from Tunis to the Gulf of Gabès), then the return trip to the north, from the Gulf of Gabès to La Seyne-sur-mer. Five stations were sampled during leg2: St15, St17, St19, St9 and St1 (Fig. 1). These stations were chosen according to different criteria of physical, biogeochemical, and biological conditions, or anthropogenic influences (see Tedetti et al., this issue). The main characteristics of stations are provided in Table 1. The SOLEMIO station (Site d'Observation Littoral pour l'Environnement du MIO) is part of the French national network of coastal observation SOMLIT (Service d'Observation en Milieu LITtoral – http://somlit.epoc.u-bordeaux1.fr/fr/). The JULIO station (JUdicious Location for Intrusions Observations) is dedicated to the study of the intrusions of Liguria current. The PEACETIME cruise (ProcEss studies at the Air-sEa Interface after dust deposition in the MEditerranean sea) took place in May-June 2017 (http://peacetime-project.org/). An extra station 'Zarzis' has been added to sampling list where biological parameters were sampled but no nutrients were measured.

Subsurface temperature and salinity were recorded continuously at high frequency all along the transect from a flow-through pumped seawater at 2-m depth, using a thermosalinograph (TSG, SeaBird SBE 21). A chamber for subsampling the flow-through seawater was plugged for automated flow cytometry measurements. At the ten fixed stations, *in situ* measurements and several operations to collect water, particles and plankton were performed (see details in Tedetti et al., this issue), including

151 the deployment of a trace metal clean carousel equipped with a conductivity-temperature-depth probe
152 (CTD; Seabird SBE 911*plus*) with ten 12-L bottles (1 Niskin, 5 Niskin-X, 4 Go-Flo). The latter allowed
153 for vertical profiles of temperature, salinity, and total chlorophyll *a* (TChl*a*) in the water column, as
154 well as seawater sampling in subsurface (5-m depth) and deep chlorophyll maximum (DCM) for
155 analysis of various parameters including nutrients, Tchl*a*, pigments, dissolved and particulate organic
156 carbon, and metallic trace elements.
157
158 **2.2. Nutrients**
159 Seawater for nutrient analyses was collected at 5-m depth and in the DCM by means of Niskin-
160 X bottles (i.e., Niskin with a completely free, Teflon coated sample chamber; model 101012X). On
161 board, in-line filtration was conducted from the Niskin-X bottles using argon pressure system (as for
162 the Go-Flo). The bottles were pressurized to 0.5 bars with argon (UN1006, compressed, 2.2) while
163 their stoppers were maintained tight by home-made high-density polyethylene (HDPE) clamps. A 10-
164 cm long piece of acid-cleaned silicon tubing was inserted into the drainage tap of the bottles, and
165 perfluoroalkoxy (PFA) filter holders (Savillex®) were connected to the tubing. Pre-combusted (450
166 °C, 6 h) glass fiber filters (GF/F, 25-mm diameter, Whatman) were placed in the filter holders. After
167 rinsing filters with several hundred mL of seawater, filtered (~ 0.7 µm) samples for nutrient analyses
168 were collected in cleaned 50-mL polycarbonate bottles and immediately stored on board at – 18 °C.
169 Samples were maintained frozen to the laboratory, where they were analysed for nutrients a few days
170 after the cruise. Nitrate (NO_3^-), nitrite (NO_2^-), phosphate (PO_4^{3-}) ions were analysed by standard
171 automated colorimetry procedure, using a Seal Analytical continuous flow AutoAnalyser III (AA3)
172 according to the protocol described by Aminot et Kérouel (2004, 2007) (detection limits of 0.05 µM
173 for NO_3^- and 0.02 µM for NO_2^- and PO_4^{3-}). Ammonium (NH_4^+) ions were analysed by fluorescence
174 according to Holmes et al. (1999) and Taylor et al. (2007).
175

176

177

178 **2.3. Automated flow cytometry**

179 The CytoSense, an automated flow cytometer (CytoBuoy b.v. (NL)) designed to study individual
180 or colonial phytoplankton cells between 0.8 and 800 µm, analysed seawater from the continuous flow-
181 through system pumped at 2-m depth, at a rate of 1 L min^{-1}, filling an intermediate 300-mL container
182 isolating the subsample to minimize the spatial extent during the analysing time. A weighted calibrated
183 peristaltic pump was used to sample the seawater and set at 5 µL s^{-1}. The sample is then surrounded
184 by a sheath loop (NaCl solution 35 ‰ filtered on 0.2 µm) to separate, align, and drive the particles to
185 the light source (laser OBIS Coherent, 488 nm, 120 mW) and was continuously recycled using a set of
186 two 0.1-µm filters. The light scattered in front of the laser beam (forward scatter, FWS) were collected
187 on two left and right photodiodes and used for laser alignment control. The light scattered orthogonally
188 (sideward scatter, SWS) and fluorescence emissions were separated by a set of optical filters (SWS,
189 488 nm), yellow fluorescence (FLY, 506–601 nm), orange fluorescence (FLO, 601–650 nm) and red
190 fluorescence (FLR, > 650 nm), and collected on photomultiplier tubes. Fluorescent beads of 3-µm
191 (Cyto-Cal™) and 10-µm (Polybead®) diameter were used every 24–72 h to normalize fluorescence
192 and size. Silica beads (Bangs lab®, silica microspheres) of 1.0, 2.02 and 3.13 µm were analysed for
193 size estimation of phytoplankton cells.

194 Ultraphytoplankton groups were optically resolved based on their light scatter and fluorescence
195 properties. Two successive samples triggered on 2 FLR signals linked to the emission of chlorophyll
196 (with values of 10 and 20 mV) were acquired, according to the frequency of the events. The
197 phytoplankton groups were classified using the Cytoclus© software. Each cell is thus characterized by
198 a set of optical pulse shapes which constitute the cytometric signature. Microsphere beads (3 µm,
199 Polyscience®) were used to discriminate between picoeukaryotes and nanophytoplankton.

Cell biovolume was estimated from a calibration relationship between different size predetermined microbeads and their equivalent cytometric forward scatter signature (FWS). The following relationships were established for picophytoplankton (Eq. 1) and nanophytoplankton (Eq. 2):

$$Log(Biovolume) = 0.2132 \times Log(FWS) - 1.161 \quad \text{(Eq. 1)}$$

$$Log(Biovolume) = 1.1104 \times Log(FWS) - 10.426 \quad \text{(Eq. 2)}$$

Eq. 2 was modified and adapted from Foladori et al. (2008) and Dugenne et al. (2016). A carbon biomass conversion was assigned to each population as follow: *Synechococcus* abundances were converted by using the estimation of 200 fg C $cell^{-1}$ (Mackey et al., 2002). Picoeukaryotes and nanoeukaryotes carbon biomass were calculated using the equation of Verity et al. (1992):

$$Qc,cal = a\ V^{0.866} \quad \text{(Eq. 3)}$$

with Qc,cal the estimated average carbon biomass per cell (in fg C $cell^{-1}$), V the biovolume (μm^3) and "a" the values of 0.39, 0.32, 0.27 and 0.25 for *Synechococcus*, picoeukaryotes, nanoeukaryotes and Cryptophytes-like, respectively. Qc,cal for each group is reported in Table 2.

The ratio between minimum and maximum mean cell biovolume (Eq. 4) has been used for the estimation of the daily growth rate (Binder et al., 1996; Vaulot and Marie, 1999). This approach assumes that the population synchronizes between growth and division phases:

$$\mu\_ratio=Log(V\_max/V\_min) \quad \text{(Eq. 4)}$$

with μ_{ratio} the daily growth rate (d^{-1}), and V_{max} and V_{min}, the minimum and maximum mean cell biovolumes (μm^3 $cell^{-1}$). The apparent increase in carbon biomass, defined as the net primary production (NPP in mg C m^{-3} d^{-1}) (Eq. 5), was calculated using the carbon conversion factor Qc,cal (Table 2) as a scalar product with N (abundance) and growth rate exponential:

$$NPP=Q\_(c,cal)\times[e\^(\mu\_ratio\ )-1]\times N \quad \text{(Eq. 5)}$$

2.4. Data analysis

A hierarchical classification was used to discriminate between the different surface water properties based on their surface temperature and salinity values. A distance matrix describing the dissimilarities of these parameters was constructed. The data were grouped using complete linkage clustering according to Euclidean (root mean squared) distances. The TS plot illustrating the different waters properties was then elaborated using the ODV 5.4.0 software developed by R. Schlitzer at the AWI. The surface water velocity for the sampled days was computed from the Copernicus service infrastructure website (https://marine.copernicus.eu/).

3. Results

3.1. Hydrological features

Subsurface temperature distribution showed a rather homogeneity during the two investigated legs (Fig. 2B), with the coldest waters being recorded in the northern stations, and the warmest towards the southern stations. This homogeneity between the two legs was also verified for the subsurface salinity distribution (Fig. 2A) with decreasing values towards the south, except a slight increase in the coastal area of the Gulf of Gabès.

The lowest temperatures, around 14 °C, were observed in the Bay of Marseille, while the highest ones were measured in the southern Tunisia coastal waters, with a maximum of 19.5 °C recorded near Djerba and Zarzis (Fig. 2B). The highest salinity values were measured in Ligurian region with a maximum of 38.50. The lowest salinity values (i.e., 37.12) were found in the northern Tunisian coastal waters, particularly in the Gulf of Tunis and in the Sicily Strait (Fig. 2A).

A hierarchical classification carried out on these subsurface temperature and salinity values allowed distinguishing 7 geographic zones (Fig. 3A, B). The colors illustrate the result of the hierarchical classification generating 7 zones (Z1 to Z7). Each zone encompassing a different number of stations: Z1, stations 1, 2, 3 and 4, Z2, station 9, Z3, stations 10 and 11, Z4, station 15, Z5, station 17, Z6, station 19, and Z7, an additional station called “Zarzis”. The temperature and salinity varied

from 13.8–15.5 °C and 38.12–38.21 in the northern basin (i.e., Z1) to 15.8–17.4 °C and 37.13–37.45 in the medium basin (i.e., Z4), and 19.2–19.9°C and 37.8–38.0 in the southern basin (i.e., Z7). For the zones in between, temperature and salinity varied for the northern part: 14.5–15.0 °C and 38.2–38.4 in Z2, 14.9–16.9 °C and 37.3–38.1 in Z3, 16.8–17.8 °C and for the southern part 37.2–37.5 in Z5, 17.8–18.7 °C and 37.5–37.7 in Z6.

The surface velocity map computed for the 8th of May 2019 (Fig. 4), corresponding to the sampling date of station 9, shows an increased water velocity southwest stations 9 and 10 likely corresponding to the edge of the seasonal northern Balearic front.

3.2. Nutrient concentrations

Nutrient concentrations measured at the 10 stations in subsurface waters (5-m depth) showed large differences between the different zones (Fig. 5): NH_4^+ varied from 0.007 to 0.790 µM, NO_3^- + NO_2^- from 0.05 to 0.63 µM, PO_4^{3-} from 0.03 to 0.34 µM, and $Si(OH)_4$ from 0.7 to 2.2 µM. Nutrient concentrations were relatively high at St4 and St9 (belonging to zones Z1 and Z2), particularly for NO_3^- + NO_2^- at St4, and $Si(OH)_4$ and PO_4^{3-} at St9. High concentration of PO_4^{3-} was also observed in zone Z6. The Redfield N / P ratio (Redfield et al., 1963) varied between 0.24 and 58. In most stations, this ratio was below 16, expressing a potential nitrogen limitation, except in St4 for which the ratio reached 58, highlighting a potential phosphorus limitation. Overall, nutrients showed decreasing concentrations towards the South (Fig. 5), the western basin being relatively mesotrophic and the eastern basin rather oligotrophic.

3.3. Distribution and composition of phytoplankton

The functional groups were resolved based on the flow cytometric optical signals from single cell biological features: FWS (i.e., Forward Scatter), SWS (i.e., Sideward Scatter), FLR (i.e., Red Fluorescence) and FLY (i.e., Yellow Fluorescence). Four groups of small plankton < 10 µm sized

275 cells) were determined according to cell optical properties (Fig. 6A, B). The plot of FLR *vs.* FLY and
276 FLR *vs.* SWS differentiated two phycoerythrin rich groups. One differentiated by high FLY
277 (phycoerythrin) emission and by small, computed size estimated of 1.05 ± 0.09 µm (Table 2) and was
278 identified as *Synechococcus.* The one presenting high FLY and computed size estimated of 5.69 ± 0.77
279 µm was identified as Cryptophytes-like. Picoeukaryotes and nanoeukaryotes cells presented high FLR,
280 low FLY emission with computed size estimated respectively of 2.45 ± 0.19 µm and 4.16 ± 0.16 µm
281 (Table 2).

282 Significant spatial heterogeneity in the distribution of ultraphytoplankton was observed
283 throughout the sampling area (Fig. 7). The total ultraphytoplankton abundance was the highest in the
284 north of the Ligurian basin (Z1 and Z2) and in the Zarzis coasts (Z7) (Fig. 7A). The highest values of
285 FLR per unit of volume, used as a proxy of Chl*a* content, were observed in zones Z1 and Z2 (Fig. 7B),
286 with a maximum of 5.10^{12} a.u. m^{-3}, and moderately high values off Zarzis (10^{12} a.u. m^{-3}). The total
287 ultraphytoplankton carbon biomass (Fig. 7C) fluctuated between 50 and 125 mg C m^{-3} in certain
288 coastal zones, such as in the south of Z7 and in the north of Z1, and up to 150 mg C m^{-3} in Z2.

289 Like the total abundance of the ultraphytoplankton (Fig. 7A), the relative abundance of each
290 group showed similar spatial distribution trends with more contrasted gradients between identified
291 zones (Fig. 8A). In general, abundances varied up to a factor of 10 from the coast of Sardinia (Z4) and
292 the Gulf of Gabès (Z5-Z6), to the northern Balearic front (Z2) and southern Tunisian coasts (Z7), as
293 shown with the *Synechococcus* which abundances varied from 3.4–9.8 10^9 cells m^{-3} to 30.8–86.9 10^9
294 cells m^{-3}. In terms of mean cell size (Fig. 8B), the zones from Z1 to Z3 in the north of the transect
295 showed larger *Synechococcus* cells (> 1 µm) and smaller picoeukaryotes and Cryptophytes-like cells
296 (< 2.5 µm / cell and < 5.5 µm / cell, respectively). The mean size distribution of nanoeukaryotes did
297 not exhibit distinguished variations and fluctuated in most waters between 3.8 and 4.6 µm.

298 The distribution of FLR per cell followed approximately that of the abundances (Fig. 8C). The
299 highest values were mainly recorded in the areas that represented the highest abundances. Its variability

within each group fluctuated in Z2 with factors of 3 for small size fractions (*Synechococcus* and picoeukaryotes), 4 for Cryptophytes-like and 5 for nanoeukaryotes.

Conversely, the maxima of abundance were synchronized with the minima in mean cell size. This pattern was particularly highlighted in Z2 (Fig. 8 and Fig. 10), especially for *Synechococcus* and picoeukaryotes with abundances varying from 30.8 to 86.9 10^9 cells m^{-3} and 1.7 to 3.8 10^9 cells m^{-3} and the mean cell size from 0.9 to 1.4 µm and 2.1 to 2.6 µm, respectively.

The nanoeukaryotes and the *Synechococcus* cells contributed the most to the FLR per unit of volume in the 7 identified zones (Fig. 9B). Their carbon biomasses (Fig. 9A) could respectively reach up to 70 and 30 mg C m^{-3}, with nanoeukaryotes as main contributors (Table 3). The coastal areas showed the highest relative contributions of nanoeukaryotes and *Synechococcus*. In the Gulf of Gabès (Z7), they were up to 51 and 22%, respectively, whereas they were about 62.1 and 19.3% in the Ligurian Basin (Z2), respectively (Table 3). The Cryptophytes-like were small contributors to total biomass, and their carbon content varied considerably among zones, being in Z2 and Z7 up to 3 times much higher than in the other areas (Table 3). The transition from coastal zone to offshore areas was followed by a reverse trend in the contribution of *Synechococcus* and picoeukaryotes to carbon biomass, where *Synechococcus* contributed more in coastal areas contrary to picoeukaryotes, contributing more offshore (Fig. 9A).

The spatial distribution of the median-normalized abundance, mean size and mean FLR_{cell} according to the identified water physical characteristics showed that three zones stand out from the others in terms of abundance, mean cell size and red FLR_{cell} (Fig. 10), namely Z1 and Z2 zones in the north of the Ligurian basin and the zone Z7 in the borders of Zarzis. These areas are characterized by relatively high abundances that may vary by a factor 10 for *Synechococcus* and Cryptophytes-like compared to the other areas (Fig. 10A). In terms of mean cell size (Fig. 10B), these same areas showed relatively smaller cells with values below the median of normalized sizes for all groups probably reflecting diurnal cell cycles that differ from one area to another. The examination of the growth rates

(Fig. 11) of the identified groups were variable among groups, the lowest growths were recorded for nanoeukaryotes, whereas the highest were for Cryptophytes-like and *Synechococcus*, with Cryptophytes-like reaching more than 2 divisions per day in Z3, Z4 and Z6. This yielded net primary production of about 36.6 mg C m^{-3} d^{-1} and 15.8 in north Mediterranean in Z2 and Z1, respectively, mostly contributed by *Synechococcus* and nanoeukaryotes, 5.8 mg C m^{-3} d^{-1} in Z4 in the central Mediterranean, and about 11 mg C m^{-3} d^{-1} in southern Mediterranean in Z6 and Z7 (Table 4).

4. Discussion

The general circulation pattern in the Mediterranean Sea western basin is characterized by the Atlantic Water (AW) transport from the Algerian Basin and spread off to the Liguro-Provencal limit thus forming the North Balearic front (Millot et al., 1991; Millot and Taupier-Letage, 2005). During this study, this hydrological structure (Fig. 4) was highlighted and corresponded to Z2 characterized by high salinity over 38.5 and low temperature between 14 and 15 °C. Like all frontal zones, high nutrient concentrations were recorded in this area particularly in terms of nitrate, silicate, and phosphate (Estrada et al., 1996). The dependence of ultraphytoplankton spatial distribution on meso or sub-meso scale hydrodynamic features like fronts that generate distinct water masses has been particularly documented in the Mediterranean Sea (Denis et al., 2010).

The part of the AW that progresses through the channel of Sardinia in its southern part (North-Tunisia vein) continues along the embankment, enters the Strait of Sicily and then in the eastern basin, going to feed the Atlantic Tunisian Current (ATC). The ATC flows eastward mainly along the 200-m isobath (Beranger et al., 2005). It splits into two branches South of Lampedusa. The first branch directly flows toward the southern part of the Levantine basin, while the second flowing over the Tunisian shelf. The later divides into two branches, the first one invades the Tunisian shelf in the Gulf of Gabès and recirculates anticyclonically on the shelf, while the second continues flowing south-eastward as an important coastal current and comes close to the Libyan coast (Jaber et al., 2014). The

salinity barrier of 37.5 characterizing the AW in the Gulf of Gabès (Bel Hassen et al., 2009) was detected at the entrance of the Gulf corresponding to Z5 (Fig. 3A), the mixing with the high salinity of the coastal waters of the Gulf makes the detection of the AW less evidenced mainly in zones Z6 and Z7.

The progressing towards the south was accompanied with a decreasing nutrient gradient mainly nitrogen and a slow increase of phosphate at station St19. The meteorological conditions during this period were characterized by a dust storm accompanied with weak rain (< 1 mm). High concentration of PO_4^{3-} observed in zone Z6, potentially due to atmospheric inputs of nutrients from a Saharan dust episode that occurred on 03/05/2019 and for which concentration of 1.06 µM was measured for PO_4^{3-} in the rainfall water collected on board. Thus, atmospheric input was a main source of phosphorus in the coastal water during dust storm (Guieu et al., 2014) and the annual input in area like the Gulf of Gabès was demonstrated to be the highest in south Mediterranean (Markaki et al., 2010; Khammeri et al., 2018). Overall, there was not an evident gradient in the abundance of the ultraphytoplankton fraction between the northern mesotrophic Mediterranean part and the southern oligotrophic part (Fig. 6). The maximum of abundance, FLR_{cell} and biomass were recorded in the Balearic frontal area (Z2), confirming that the large-scale phytoplankton distribution in the Mediterranean was specifically affected by hydrodynamics (Casotti et al., 2003; Denis et al., 2010). This area was particularly rich in silicate and phosphate and exhibited the highest abundance of larger size fractions (nanoeukaryotes and Cryptophytes-like) ($P < 0.05$ and $R^2 > 0.7$) (Fig. 7), confirming that low nutrient regions are dominated by small phytoplankton, mostly *Synechococcus*, *Prochlorococcus* and picoeukaryotes, whereas more productive regions support not only these small cells but also abundances of larger species (Raimbault et al., 1998; Hirata et al., 2011).

Synechococcus were by far the most abundant group in all prospected zones, its highest relative biomass was reached in the Gulf of Gabès (Table 3). *Prochlorococcus* were not resolved in our study. The nonresolution of *Prochlorococcus* in subsurface water using a CytoSense could be related to their

dim fluorescence signature due to high light intensity affecting surface waters in April-May, combined to a high background noise in the sheath fluid as no coal filter was used to lower the trigger level as it has been shown to greatly improve the resolution of this group (Marrec et al., 2018). Nevertheless, the analysis of samples from the DCM using the same instrument showed the presence of *Prochlorococcus* at depth below 50 m (data not shown). This is consistent with previous patterns observed along the Tunisian coasts with the presence of *Prochlorococcus* at warm and stratified water more than 60 m in depth (Khemmari et al., 2020; Quéméneur et al., 2020). Nonetheless, this dominance of *Synechococcus* over *Prochlorococcus* already reported in the Mediterranean confirms the statement that *Synechococcus* is more adapted to the general hydrodynamic and nutrient conditions in the Mediterranean Sea (Denis et al., 2010).

Synechococcus mean estimated size and associated biovolume of 1.05 ± 0.09 µm and 0.6 ± 0.17 µm^3, respectively (Table 2), were in the same range of 0.8 to 1.2 µm and 0.25 to 1.00 µm^3, respectively reported in previous studies (Morel et al., 1993; Shalapyonok et al., 2001; Sosik et al., 2003; Hunter-Cevera et al., 2014; Marrec et al., 2018). Relatively smaller *Synechococcus* cells with values below the median of normalized sizes were observed in the low latitude and warm southern Tunisian waters (Fig. 9B), confirming that their distribution appears to be principally controlled by water temperature and latitude (Pittera et al., 2014). A likely genomic differentiation within this group could also be suggested, although a dominance of the clade III has been reported in the Mediterranean Sea, but this did not exclude an ecologically meaningful fine-scale diversity within currently defined *Synechococcus* clades (Farrant et al., 2016).

The mean size of the main nanoeukaryotes functional group observed was 4.15 ± 0.16 µm (Table 2). This is consistent with the value of 4.1 ± 0.5 µm reported by Marrec et al. (2018) in the north-western Mediterranean Sea. No significant variations in the mean size of nanoeukaryotes along the transect was observed (Fig. 9B) suggesting that this community might be dominated by similar genera. Indeed, the major feature of the Mediterranean basin in various regions and season is a biomass

400 dominated by Prymnesiophytes (Latasa et al., 1992; Claustre et al., 1994; Bustillos-Guzman et al.,
401 1995; Vidussi et al., 2000) with the genus Chrysochromulina (3.2–4.0 µm) largely represented in the
402 north-western Mediterranean (Percopo et al., 2011). Conversely, the contribution of Prymnesiophytes
403 to chlorophyll biomass considered as prominent feature in the Mediterranean was rather low in the
404 Gulf of Gabès (Bel Hassen et al., 2008; 2009a) and mainly explained by the dominance of smaller
405 chlorophyll b containing nanoplankton like prasinophytes. Nanoeukaryotes were the main contributors
406 (> 60 %) in terms of pigment content (defined by FLR) and carbon biomass. The contribution of nano
407 and picoeukaryotes in terms of pigment fluctuated between 80 and 84% in central Mediterranean, and
408 between 69 and 77% in both northern and southern Mediterranean (Table 3), where the prokaryotes
409 (*Synechococcus*) exhibited their highest contribution (between 15 to 18.9% of FLR). This is less than
410 the prokaryotes contribution (32 to 47%) to total Chl*a* reported using chemotaxonomic approach by
411 Barlow et al. (1997) in the southern Mediterranean region and the ranges of 26 and 28% found by Bel
412 Hassen et al. (2009a) in the Gulf of Gabès during spring and summer, respectively. These deviations
413 could be in part explained by the presumed contribution of *Prochlorococcus*, not resolved in our case
414 in surface water. Indeed, when comparing the only contribution of *Synechococcus* in the Gulf of Gabès
415 (15-17%) (Table 3) we found consistent values (15% in mean) with what reported using
416 chemotaxonomic approach in the same area for the same period (Bel Hassen et al., 2009a).
417 The growth rate, estimated from the difference in minimal and maximal values of biovolume,
418 showed that the highest rates were observed for the orange fluorescing phycoerythrin containing cells,
419 i.e., Cryptophytes-like and *Synechococcus*. The *Synechococcus* growth rate estimates fluctuated
420 between 0.38 and 1.1 d^{-1}. This was consistent with values of 0.48–0.96 d^{-1} reported by Ferrier-Pages
421 and Rassoulzadegan (1994) and with the value of 0.49 d^{-1} reported in the north-western Mediterranean
422 Sea (Marrec et al., 2018). Cryptophytes-like growth rates showed their highest variability (0.3-1.7 d^{-1})
423 in Z1 but is still consistent with the rate of 0.75 d^{-1} determined in spring 2004 in the center of the
424 Liguro-Provencal basin (Gutierrez-Rodriguez et al., 2010). The yielded *Synechococcus* apparent NPP

rates showed their highest values in Z1 (1.3-12 mg C m^{-3} d^{-1}) and Z2 (13.9-23 mg C m^{-3} d^{-1}), combined with high abundances recorded in these areas. These NPP were higher than the range of 0.01-1 mg C m^{-3} d^{-1} reported by the study of Agawin et al. (1998) by means of a biovolume to C conversion over the course of 1997-1998 (February to May), and also the value of 2.68 mg C m^{-3} d^{-1} reported by Marrec et al. (2018) in north-western Mediterranean Sea during fall season. These studies used different approximations to calculate the biovolume to cellular carbon content. However, it has been demonstrated by Marrec et al. (2018) that cyanobacteria NPP rates obtained from different calculations provides similar specific C uptake rates suggesting that these populations follow a daily dynamic at equilibrium. Nanoplankton was expected to be the main contributor to the NPP because of its high abundance and high cellular carbon content (Table 3), but its relative low growth rates generally under 0.3 d^{-1}, even lower than the range (0.48-2.4 d^{-1}) reported in north-western Mediterranean (Ferrier-Pages and Rassoulzadegan, 1994), could explain this low NPP particularly in central Mediterranean and in the northern Tunisian coasts. It is worth noting that NPP estimation does not accommodate any cells removal processes that could be caused by grazing or physical transport. Even if this estimation is valuable for all the resolved groups, nevertheless the grazing pressure on nanoplankton and its motile capabilities are largely underestimated. Indeed, an active top-down control of ultraphytoplankton was largely suspected in the southern Tunisian coasts (Hamdi et al., 2015; Khammari et al., 2020) preventing from nanoeukaryotes accumulations. Moreover, the approach used for the calculation of the growth rate based on the ratio between max and minimum cell biovolume (Binder et al., 1996; Vaulot and Marie, 1999) assumes that cell growth and division are separated in time (synchronous population), whereas these processes occur simultaneously in a population. The growth rates calculation based on cell size distribution allowed for superior estimation than using the ratio Log(Vmax/Vmin), especially for asynchronized populations like nanoeukaryotes and Cryptophytes-like. The picoeukaryotes NPP varied between 0.48 to 19 mg C m^{-3} d^{-1}, which is consistent with range

449 of picoplankton production rates of 2.2–19.6 mg C m^{-3} d^{-1} compiled by Magazzu and Decembrini
450 (1995) in the Mediterranean Sea.

451 Except the Gulf of Gabès (Z6 and Z7), which is submitted to atmospheric forcing events, a
452 decreasing gradient in the NPP was observed along the North-South transect, confirming this general
453 trend in the Mediterranean, based on the whole phytoplankton size population (Colella et al., 2003).
454 The size fractioned NPP assessment conducted in the present study focused on the size under < 10 µm,
455 demonstrated to represent 20% of NPP measured by ^{14}C particulate organic carbon production rates in
456 a NW coastal Spanish station (Cermeno et al., 2006). The focus on this size fraction is justified by
457 their high accumulation capabilities of contaminants (see this issue). The determination of the groups
458 that present the high carbon assimilation could provide an important insight into the characterization
459 of the phytoplankton mostly involved in the contaminant transfer in the trophic chain.

460

461 **5. Conclusions**

462 The monitoring of the subsurface ultraphytoplankton at high frequency along a North-South
463 Mediterranean round-trip transect highlighted the following conclusions:

464 - The Balearic frontal region showed the highest abundances and biomasses mostly attributed to
465 *Synechococcus* and nanoplankton. The productivity was mostly sustained by *Synechococcus*.
466 This pattern confirms the general statement that hydrodynamics is an important factor shaping
467 the structure of this ultraphytoplanktonic community.
468 - *Synechococcus* was by far the most abundant group in subsurface water with high biomass
469 concentration in the coastal zones, reaching up to 22% in the Gulf of Gabès.
470 - Nanoplankton represented up to 51% of the total ultraphytoplankton biomass in all zones. If
471 we consider that the transfer of contaminants to phytoplankton species is mainly biomass
472 related, nanoplankton will be the relevant group to monitor. The straight conclusion coming
473 out from this result is that the southern Tunisian coasts, with the lowest nanoplanktonic

biomasses, were probably the ecosystem that accumulates the least contaminants in its trophic chain

- In almost all zones, the highest carbon turnover was ensured by *Synechococcus*. Its contribution to the contaminant transfer to higher trophic levels is largely dependent on the potential grazing activities.

Acknowledgements. The MERITE-HIPPOCAMPE cruise was organised and supported by the French Oceanographic Fleet (FOF), CNRS/INSU, IFREMER, IRD, the Ministry of Agriculture, Hydraulic Resources and Fisheries of Tunisia, and the Ministry of Higher Education and Scientific Research of Tunisia. It was funded by the "Pollution & Contaminants" transverse axis of the CNRS-INSU MISTRALS program, as well as the IRD French-Tunisian International Joint Laboratory (LMI) "COSYS-Med", the Action Sud and Transverse Axis programs of the MIO, the Ocean Department of IRD, and IFREMER. The MERITE-HIPPOCAMPE cruise represented a joint action of the MERITE-MERMEX and CHARMEX projects of MISTRALS, the LMI "COSYS-Med" and the "CONTAM" Transverse Axis of the MIO. We are grateful to the principal investigators (PIs) of the MERITE-HIPPOCAMPE project, J. Tronczynski (IFREMER), M. Tedetti, F. Carlotti, M. Pagano and C. Garnier (MIO), as well as the captain and crew of the R/V *Antéa* for their help and assistance during the cruise. We thank C. Sammari and INSTM, the IRD representation in Tunisia, and the French Institute of Tunisia for their logistic and financial assistance in the preparation of the cruise. We acknowledge the Service Atmosphère-Mer (SAM) of the MIO, particularly D. Malengros, for the preparation and management of the embarked material, the Plateforme Analytique de Chimie des Environnements Marins (PACEM platform) of the MIO for nutrient analyses, and K. Desboeufs (LISA) for providing concentrations of nutrients in rainwater samples.

References

Alekseenko, E., Roux, B., Sukhinov, A., Kotarba, R., and Fougere, D., (2013). Coastal hydrodynamics in a windy lagoon. Comput. Fluids 77, 2435.

Aminot, A., Kérouel, R., (2004). Hydrologie des écosystèmes marins. Paramètres et analyses Ed. Ifremer, 336 p.

Aminot, A. and Kérouel, R, (2007). Dosage Automatique des Nutriments Dans Les Eaux Marines: Méthodes en Flux Continu, Edition Quae, Ifremer, Plouzané, France.

Ayata, S.D., Irisson, J.O., Aubert, A., Berline, L., Dutay, J.C., Mayot, N., Nieblas, A.E., D'Ortenzio, F., Palmieri, J., Reygondeau, G., Rossi, V., Guieu, C., (2018). Regionalisation of the Mediterranean basin, a MERMEX synthesis. Progress in Oceanography, 163, 7–20. doi: 10.1016/j.pocean.2017.09.016.

Bel Hassen, M., Drira, Z., Hamza, A., Ayadi, H., Akrout, F., Issaoui, H., (2008). Summer phytoplankton pigments and community composition related to water massproperties in the Gulf of Gabes. Estuarine, Coastal and Shelf Science 77,645–656.

Barlow, R.G., Mantoura, R.F.C., Cummings, D.G., Fileman, T.W., (1997). Pigmentchemotaxonomic distributions of phytoplankton during summer in the western Mediterranean. Deep-Sea Research II 44, 833–850

Bel Hassen, M., Drira, Z., Hamza, A., Ayadi, H., Akrout, F., Messaoudi, S., Issaoui, H.,Aleya, L., Bouaı̈n,A., (2009a). Phytoplankton dynamics related to water massproperties in the Gulf of Gabes: Ecological implications. Journal of MarineSystems 75, 216–226.

Bel Hassen M., Hamza A., Drira Z., Zouari A., Akrout F., Messaoudi S., Aleya L., Ayadi H., (2009b). Phytoplankton-pigment signatures and their relationship to springΓÇôsummer stratification in the Gulf

of Gabes, Estuarine, Coastal and Shelf Science, Volume 83, Issue 3, Pages 296-306, ISSN 0272-7714, https://doi.org/10.1016/j.ecss.2009.04.002.

Béranger, K., Mortier, L., Gasparini, G.P., Gervasio, L., Astraldi, M., Crepon, M., (2004). The dynamics of the Sicily Strait: a comprehensive study from observations andmodels. Deep-Sea Research II 51, 411–440.

Binder, B. J., Chisholm, S. W., Olson, R. J., Frankel, S. L., and Worden, A. Z, (1996). Dynamics of picophytoplankton, ultraphytoplankton and bacteria in the central equatorial Pacific, Deep-Sea Res. Pt.II, 43, 907–931.

Brewin, R. J. W., Sathyendranath S., Hirata T., Lavender S. J., Barciela R. M., and Hardman-Mountford N. J., (2010). A three-component model of phytoplankton size class for the Atlantic Ocean, *Ecological Modelling*, *221*, 1472– 1483.

Brosnahan, M. L., Velo-suarez L., Ralston D. K., Fox S. E., Sehein T. R., Shalapyonok A., Sosik H. M., Olson R. J., and Anderson D. M., (2015). Rapid growth and concerted sexual transitions by a bloom of the harmful dinoflagellate *Alexandrium fundyense (*Dinophyceae), *Limnol. Oceanogr.*, *60*, 2059–2078.

Bustillos-Guzmán, J., Claustre H. & Marty J.C., (1995). Specific phytoplankton signatures and their relationship to hydrographic conditions in the coastal northwestern Mediterranean Sea. Mar. Ecol. Prog. Ser. 124: 247-258.

Campbell, L., Olson, R. J., Sosik, H. M., Araham, A., Henrichs, D. W., Hyatt, C. J., et al., (2010). First harmful Dinophysis (Dinophyceae, Dinophysiales) bloom in the U.S is revealed by automated imaging flow cytometry. J. Phycol. 46, 66-75.

Casotti, R., A. Landolfi, C. Brunet, F. D'Ortenzio, O. Mangoni and M. Ribera D'Alcala, (2003). Composition and dynamics of the phytoplankton of the Ionian Sea (eastern Mediterranean), *J. Geophys. Res.*, *108* (9), 1–19.

Cermeno, P., Maranon E., Perez V., Serret P., Fernandez E., and Castro C. G., (2006). Phytoplankton size structure and primary production in a highly dynamic coastal ecosystem (Ria de Vigo, NW-Spain): Seasonal and short-time scale variability, *Estuarine, Coastal and Shelf Science*, *67*, 251–266.

Chavez, F.P., Messié, M., Pennington, J.T., (2011). Marine primary production in relation to climate variability and change. Annual Review of Marine Science, 3, 227–260. doi: 10.1146/annurev.marine.010908.163917

Chouvelon, T., Strady, E., Harmelin-Vivien, M., Radakovitch, O., Brach-Papa, C., Crochet, S., Knoery, J., Rozuel, E., Thomas, B., Tronczynski, J., Chiffoleau, J.F., (2019). Patterns of trace metal bioaccumulation and trophic transfer in a phytoplankton-zooplankton-small pelagic fish marine food web, Marine Pollution Bulletin, 146, 1013–1030. doi: 10.1016/j.marpolbul.2019.07.047.

Claustre, H., Kerhervé, P., Marty, J. C., Prieur, L., Videau, C., and Hecq, J.-H., (1994). Phytoplankton dynamics associated with a geostrophic front: ecological and biogeochemical implications, J. Mar. Res., 52, 711–742.

Colella S., D'Ortenzio F., Marullo S., Santoleri R., Ragni,M. and Ribera M. d'Alcala, (2004). Primary production variability in the Mediterranean Sea from SeaWiFS data", Proc. SPIE 5233, Remote Sensing of the Ocean and Sea Ice 2003. https://doi.org/10.1117/12.516791.

Denis, M., Thyssen M., Martin V., Manca B.,.and Vidussi F., (2010). Ultraphytoplankton basin-scale distribution in the eastern Mediterranean Sea in winter: link to hydrodynamism and nutrients, *Biogeosciences*, *7*, 2227–2244.

Dugenne, M, (2017). Dynamique du phytoplancton en mer Méditerranée: Approches par mesures à haute fréquence, modélisation, et statistiques bayésiennes, PhD Thesis, Aix Marseille Université, available at:http://www.theses.fr/s137171(last access: 7 March 2018).

Dugenne, M., Thyssen M., Garcia N., Mayot N., Bernard G., and Grégori G. J., (2015). Monitoring of a potential harmful algal species in the Berre lagoon by automated *in situ* flow cytometry, *HJ Ceccaldi*

et al. (eds), Marine Productivity: Perturbations and Resilience of Socio-ecosystems, Springer 2015, 117–126.

DuRand, M. D., Olson, R. J., and Chisholm, S. W. (1996). Phytoplankton population dynamics at the Bermuda Atlantic Time-series station in the Sargasso Sea, Deep-Sea Res. Pt. II, 48, 1983–2003, 2001.

Estrada, M.: Primary production in the northwestern Mediterranean, Sci. Mar., 60, 55–64.

Estrada, M. (1996). Primary production in the northwestern Mediterranean, *Scientia Marina*, *60* (2), 55–64.

Falkowski, P.G., Barber, R.T., Smetacek, V.V., (1998). Biogeochemical Controls and Feedbacks on Ocean Primary Production. Science, 281, 200–207. doi: 10.1126/science.281.5374.200

Farrant, G. K., Doré, H., Cornejo-Castillo, F. M., Partensky, F., Ratin, M., Ostrowski, M., Pitt, F. D., Wincker, P., Scanlan, D. J., Iudicone, D., Acinas, S. G., and Garczarek, L., (2016). Delineating ecologically significant taxonomic units from global patterns of marine picocyanobacteria, P. Natl. Acad. Sci. USA, 113, 3365–3374, https://doi.org/10.1073/pnas.1524865113.

Ferrier-Pages, C. and Rassoulzadegan, F., (1994). Seasonal impact of the microzooplankton on pico- and nanoplankton growth rates in the northwest Mediterranean Sea, Mar. Ecol.-Prog. Ser., 108, 283–294.

Field, C. B., (1998). Primary production of the biosphere: integrating terrestrial and oceanic components, Science, 281, 237–240, https://doi.org/10.1126/science.281.5374.237.

Foladori, P., Quaranta, A. and Ziglio, G. (2008). Use of silica microspheres having refractive index similar to bacteria for conversion of flow cytometric forward light scatter into biovolume, *Water Res.*, *42*, 3757–3766.

Goldman, J. C., McCarthy, J. J. and Peavey, D. G., (1979). Growth rate influence on the chemical composition of phytoplankton in oceanic waters, *Nature*, *279*, 210–215.

Guieu, C., Aumont, O., Paytan, A., Bopp, L., Law, C. S., Mahowald,N., Achterberg, E. P., Marañón, E., Salihoglu, B., Crise, A., Wa-gener, T., Herut, B., Desboeufs, K., Kanakidou, M., Olgun, N.,Peters,

F., Pulido-Villena, E., Tovar-Sanchez, A., and Völker, C., 2014. The significance of the episodic nature of atmospheric depositionto Low Nutrient Low Chlorophyll regions, Global Biogeochem.Cy.

Gutierrez-Rodriguez, A., Latasa M., Estrada M., Vidal M., and Marrase C., 2010. Carbon fluxes through major phytoplankton groups during the spring bloom and post-bloom in the Northwestern Mediterranean Sea, *Deep-Sea Research I*, *57*, 486–509.

Hamdi, I., Denis, M., Bellaaj-Zouari, A., Khemakhem, H., Hassen, M. B., Hamza, A., et al., (2015). The characterisation and summer distribution of ultraphytoplankton in the Gulf of Gabès (Eastern Mediterranean Sea, Tunisia) by using flow cytometry. Cont. Shelf Res. 93, 27–38. doi: 10.1016/j.csr.2014.10. 002

Holmes, R.B., Aminot, A., Kérouel, R., Hooker, B.A., Peterson, B.J., 1999. A simple and precise method for measuring ammonium in marine and freshwater ecosystems Can. J. Fish. Aquat. Sci. 56, 1801–1808.

Hirata, T., Hardman-Mountford N. J., Brewin R. J. W., Alken J., Barlow R., Suzuki K., Isada T., Howell E., Hashioka T., Noguchi-Aita M., and Yamanaka Y., 2011. Synoptic relationships between surface chlorophyll-a and diagnostic pigments specific to phytoplankton functional types, *Biogeosciences*, *8*, 311–327.

Hunter-Cevera, K. R., Neubert, M. G., Solow, A. R., Olson, R. J., Shalapyonok, A., and Sosik, H. M., 2014. Diel size distributions reveal seasonal growth dynamics of a coastal phytoplankter, P. Natl. Acad. Sci. USA, 111, 9852–9857, https://doi.org/10.1073/pnas.1321421111.

Jaber, I.B., Abdennadher, J., Boukthir, M., 2014. Pathways of the modified Atlantic wateracross the Strait of Sicily. Geophys. J. 36 (4), 75–84.

Khammeri, Y., Bellaaj-Zouari, A., Hamza, A., Medhioub, W., Sahli, E., Akrout, F., et al., 2020. Ultraphytoplankton community composition in Southwestern and Eastern Mediterranean Basin: relationships to water mass properties and nutrients. J. Sea Res. 158:101875. doi: 10.1016/j.seares.2020.101875

Khammeri, Y., Hamza, I.S., Bellaej-Zouari, A., Hamza, A., Sahli, E., Akrout, F., Messaoudi, S., Belhassen, M., 2018. Atmospheric bulk deposition of dissolved nitrogen, phosphorus and silicate in the Gulf of Gabès (South Ionian Basin); implications for marine heterotrophic prokaryotes and ultraphytoplankton. Con. Shel. Res. 159, 1–11. https://doi.org/10.1016/j.csr.2018.03.003.

Latasa, M., Estrada, M. and Delgado, M., 1992. Plankton pigment relationships in the Northwestern Mediterranean during stratification, *Mar. Ecol. Progr. Ser., 88*, 61-73.

Marina L., 2003. Mesoscale variability of phytoplankton and of new production : Impact of the large scale nutrient distribution. Journal of Geophysical Research, American Geophysical Union, 108 (C11), pp.3358. ff10.1029/2002JC001577ff. ffhal-00153678

Mackey, D.J., Blanchot, J., Higgins, H.W., Neveux, J., 2002. Phytoplankton abundances and community structure in the equatorial Pacific. Deep Sea Res. 49 (13–14), 2561–2582. https://doi.org/10.1016/S0967-0645(02)00048-6.

Magazzu, G. and F. Decembrini, 1995. Primary production, biomass and abundance of phototrophic picoplankton in the Mediterranean Sea: a review, *Aquat. microb. Ecol., 9*, 97–104.

Markaki, Z., Loye-Pilot, M.D., Violaki, K., Benyahya, L., Mihalopoulos, N., 2010. Variability of atmospheric deposition of dissolved nitrogen and phosphorus in the Mediterranean and possible link to the anomalous seawater N/P ratio. Mar. Chem. 120 (1–4), 187–194. https://doi.org/10.1016/j.marchem.2008.10.005

Marrec, P., Grégori, G., Doglioli, A. M., Dugenne, M., Della Penna, A., Bhairy, N., Cariou, T., Hélias Nunige, S., Lahbib, S., Rougier, G., Wagener, T., and Thyssen, M., 2018. Coupling physics and biogeochemistry thanks to high-resolution observations of the phytoplankton community structure in the northwestern Mediterranean Sea, Biogeosciences, 15, 1579–1606, https://doi.org/10.5194/bg-15-1579-2018.

Millot C., 1991. Mesoscale and seasonal variahility of the circulation in the western Mediterranean. Dynamics of Atmospheres and Oceans. 15, 170-214.

Millot, C. and Taupier-Letage, I., 2005.Circulation in the Mediterranean Sea, The Mediterranean Sea, The Handbook of Environ. Chem., Springer Berlin, Heidelberg, 323–334.

Morel. A, Ahn, Y, Partensky, F., Vaulot, D., Claustre, H., 1993. Proch1orococcus and Synechococcus: a comparatlve study of then optlcal properties ln relation to their size and pigmentation. J. mar. Res, 51: 617-649

Nizzetto, L., Gioia, R., Li, J., Borgå, K., Pomati, F., Bettinetti, R., Dachs, J., Jones, K.C., 2012. Biological pump control of the fate and distribution of hydrophobic organic pollutants in water and plankton. Environ. Sci. Technol. 46 (6), 3204–3211.

Percopo, I., Siano, R., Cerino, F., Sarno, D., and Zingone, A, 2011. Phytoplankton diversity during the spring bloom in the northwestern Mediterranean Sea, Bot. Mar., 54, 243–267, https://doi.org/10.1515/bot.2011.033.

Pittera, J., Humily, F., Thorel, M., Grulois, D., Garczarek, L., and Six, C., 2014. Connecting thermal physiology and latitudinal niche partitioning in marine Synechococcus, ISME J., 8, 1221–1236, https://doi.org/10.1038/ismej.2013.228.

Pulido-Villena, E., Baudoux, A.-C., Obernosterer, I., Landa, M.,Caparros, J., Catala, P., Georges, C., Harmand, J., and Guieu,C, 2014. Microbial food web dynamics in response to a Saha-ran dust event: results from a mesocosm study in the olig-otrophic Mediterranean Sea, Biogeosciences Discuss., 11, 337–371, doi:10.5194/bgd-11-337-2014.

Quéméneur M, Bel Hassen M, Armougom F, Khammeri Y, Lajnef R, Bellaaj-Zouari A., 2020. Prokaryotic Diversity and Distribution Along Physical and Nutrient Gradients in the Tunisian Coastal Waters (South Mediterranean Sea). Front Microbiol. Dec 1; 11:593540. doi: 10.3389/fmicb.2020.593540. PMID: 33335519; PMCID: PMC7735998.

Redfield, A.C., Ketchum, B.H., Richards, F.A., 1963. The influence of organisms in the composition of seawater. In : Hill, M.N. (Ed.), The sea, Vol II. Wiley,New York, pp. 26–77.

Ribalet, F., Swalwell, J., Clayton, S., Jiménez, V., Sudek, S., Lin, Y., Johnson, Z. I., Worden, A. Z., and Armbrust, E. V., 2015. Light-driven synchrony of Prochlorococcus growth and mortality in the subtropical Pacific gyre, P. Natl. Acad. Sci. USA, 112, 8008–8012, https://doi.org/10.1073/pnas.1424279112.

Raimbault, P-, Rodier, M., Taupier-Letage, I., 1988. Size fraction of phytoplankton in the Ligurian Sea and the Algerian Basin (Mediterranean Sea): size distribution versus total concentrahon. Mar. Microb. Food Webs. (In press)

Sakka, H.A., Niquil, N., Legendre, L., 2014. Planktonic food webs revisited: Reanalysis of results from the linear inverse approach. Prog. Ocea. 120, 216–229. https://doi.org/ 10.1016/j.pocean.2013.09.003.

Shalapyonok, A., Olson, R. J., and Shalapyonok, L. S.,2001. Arabian Sea phytoplankton during Southwest and Northeast Monsoons 1995: composition, size structure and biomass from individual cell properties measured by flow cytometry, Deep-Sea Res. Pt. II, 48, 1231–1261.

Siegenthaler, U., and Sarmiento J. L., 1993. Atmospheric carbon dioxide and the ocean, *Nature*, *365*, 119–125.

Sobek, A., Gustafsson, O., 2004. Latitudinal fractionation of polychlorinated biphenyls in surface seawater along a 62°N–89°N transect from the southern Norwegian Sea to the North Pole area. Environ. Sci. Technol. 38, 2746–2751.

Sosik, H. M., Olson, R. J., Neubert, M. G., Shalapyonok, A., and Solow, A. R.,2003. Growth rates of coastal phytoplankton from time-series measurements with a submersible flow cytometer, Limnol. Oceanogr., 48, 1756–1765, https://doi.org/10.4319/lo.2003.48.5.1756.

Steele, J. H., 1962. Environmental control of photosynthesis in the sea, *Limnol. Oceanogr.*, *7*, 137–150.

693 Taylor, B.W., Keep, C.F., Hall, R.O., Koch, B.J., Tronstad, L.M., Flecker, A.S., and Ulseth, A.J., 2007.
694 Improving the fluorometric ammonium method: matrix effects, background fluorescence, and standard
695 additions. Journal of the North American Benthological Society 26, 167-177.
696 Tedetti, M., Tronczynski, J., 2019. HIPPOCAMPE cruise, RV Antea,
697 https://doi.org/10.17600/18000900
698 Tedetti, M., et al. Contamination of planktonic trophic webs in the Mediterranean Sea: Introduction to
699 the MERITE-HIPPOCAMPE oceanographic cruise (spring 2019). In preparation, this issue.
700 Vaulot, D. and Marie, D., 1999. Diel variability of photosynthetic picoplankton in the equatorial
701 Pacific, J. Geophys. Res.-Oceans, 104, 3297–3310, https://doi.org/10.1029/98JC01333.
702 Verity, P. G., Robertson C. Y., Tronzo C. R., Andrews M. G., Nelson J. R., and Sieracki M. E., 1992.
703 Relationships between cell volume and the carbon and nitrogen content of marine photosynthetic
704 nanoplankton, *Limnol.Oceanogr.*, *37* (7), 1434–1446.
705 Vidussi, F., Marty J-C., and Chiavérini J., 2000. Phytoplankton pigment variations during the transition
706 from spring bloom to oligotrophy in the northwestern Mediterranean Sea, *Deep-Sea Research I*, *47*,
707 423–445.
708 Vidussi, F., Claustre, H., Manca, B. B., Luchetta, A., and Marty, J.-C., 2001. Phytoplankton pigment
709 distribution in relation to upper thermocline circulation in the eastern Mediterranean Sea during
710 winter, *J. Geophys. Res.*, 106(C9), 19939– 19956, doi:10.1029/1999JC000308.
711 Wallberg, P., Bergqvist, P.A., Anderson, A., 1997. Potential importance of protozoan grazing on the
712 accumulation of polychlorinated biphenyls in the pelagic food web. Hydrobiologia 357, 53–62.
713 Zhou, Q., W. Chen, H. Zhang, L. Peng, L. Liu, Z. Han, N. Wan, L. Li and L. Song, 2012. A flow
714 cytometer-based protocol for quantitative analysis of bloom forming cyanobacteria (*Microcystis*) in
715 lake sediments, *J. of Env. Sciences*, *24* (9), 1709–1716.
716
717

Table 1. Main characteristics of the ten stations sampled along a North-South Mediterranean transect during the MERITE-HIPPOCAMPE cruise (13 April-14 May 2019). (a) The SOLEMIO station (Site d'Observation Littoral pour l'Environnement du MIO) is part of the French national network of coastal observation SOMLIT (Service d'Observation en Milieu LITtoral – http://somlit.epoc.u-bordeaux1.fr/fr/). (b) The JULIO station (JUdicious Location for Intrusions Observations) is dedicated to the study of the intrusions of Liguria current. (c) The PEACETIME cruise (ProcEss studies at the Air-sEa Interface after dust deposition in the MEditerranean sea) took place in May-June 2017 (http://peacetime-project.org/) (d) Consensus ecoregions of the Mediterranean Sea as defined by Ayata et al. (2018).

Station	Latitude (N)	Longitude (E)	Location	Characteristics	Depth (m)	Period
St2	42° 56.020'	5° 58.041'	Toulon – offshore (Maures Escarpement)	Limit of the continental shelf; Boundary of the Ligurian ecoregion[d]	1770	14-16/04
St4	43° 14.500'	5° 17.500'	Bay of Marseille (SOLEMIO[a] station)	Urbanized bay	58	16-18/04
St3	43° 08.150'	5° 15.280'	Marseille – offshore (JULIO[b] station)	Southeast entrance to the Gulf of Lion; Liguria current intrusions	95	18-20/04
St10	40° 18.632'	7° 14.753'	Offshore (PEACETIME[c] 2 station)	Near the North thermal front of the Balearic Islands	2791	22-24/04
St11	39° 07.998'	7° 41.010'	Offshore (PEACETIME[c] 3 station)	Algerian ecoregion[d]; Gyres, intermediate primary production	1378	25-26/04
St15	36° 12.883'	11° 07.641'	Gulf of Hammamet	Phytoplankton area and high density of small pelagic fishes	100	29-30/04
St17	34° 30.113'	11° 43.573'	Boundary Gulf of Gabes	Gabès ecoregion[d] boundary; High density of small pelagic fishes	48	01-02/05
St19	33° 51.659'	11° 18.509'	Gulf of Gabes – South	Gabès ecoregion[d]; High density of small pelagic fishes and phytoplankton area	50	02-05/05
St9	41° 53.508'	6° 19.998'	Offshore (PEACETIME[c] 1 station)	Ligurian ecoregion[d] boundary	2575	08-09/05
St1	43° 03.819'	5° 59.080'	Bay of Toulon	Urbanized bay	91	10-11/05
Zarzis	33° 37.952'	11° 17.73'	Zarzis	Saharan dust deposit	30	03-04/05

Table 2. Mean and SD of FWS, estimated size and biovolume of the Synechoccocus, picoeukaryotes, nanoeukaryotes and Cryptophytes-like

(1) Verity et al. (1992), (2) Campbell et al. (1994) and Shalapyonok et al. (2001), (3) Marrec et al. (2018)

Parameters	Synechoccocus	Picoeukaryotes	Nanoeukaryotes	Cryptophytes-like
FWS (a.u. cell^{-1})	292.4 ± 110	6078 ± 1480	34200 ± 4395	91200 ± 47049
Estimated size (µm)	1.05 ± 0.09	2.46 ± 0.19	4.15 ± 0.16	5.59 ± 0.77
Biovolume (µm^3 cell^{-1})	0.60 ± 0.17	7.76 ± 1.72	37.43 ± 4.36	91.47 ± 42.12
Conversion coefficients (a,b)	(0.39,0.86)[1]	(0.32,0.8666)[1]	(0.27,0.8666)[1]	(0.25,0.8666)[1]
Calculated Qc,cal (fg C cell^{-1})	253	1871	6258	12273
Literature Qc (fg C cell^{-1})	100[(3)]-250[(2)]	2108[(2)]	9000[(3)]	-

Table 3. Community contribution by zone in terms of abundance (cells cm^{-3}), biomass (µg C m^{-3}) and total FLR (a.u. cm^3) (Syn= *Synechococcus*, Pico= picoeukaryotes, Nano=nanoeukaryotes, Cry=Cryptophytes-like)

Zone	Abundance (%)				Biomass (%)				Red fluorescence (%)			
	Syn	***Pico***	***Nano***	***Cry***	***Syn***	***Pico***	***Nano***	***Cry***	***Syn***	***Pico***	***Nano***	***Cry***
Z1	79.2 *±15.5*	7.5 *±10.1*	11.6 *±6.4*	0.7 *±0.3*	19.3 *±17.6*	11.1 *±5.5*	62.1 *±13.5*	7.0 *±2.0*	18.9 *±15.0*	8.3 *±3.2*	60.9 *±9.7*	8.4 *±6.4*
Z2	80.6 *±14.2*	5.3 *±4.8*	12.9 *±9.4*	1.7 *±0.4*	17.1 *±10.3*	6.4 *±2.9*	63.9 *±10.5*	12.6 *±3.4*	9.9 *±7.8*	3.8 *±2.4*	73.2 *±8.1*	12.9 *±3.5*
Z3	59.1 *±18.8*	18.5 *±6.7*	19.7 *±13.1*	0.6 *±0.3*	7.7 *±5.4*	19.2 *±4.3*	68.5 *±8.3*	3.6 *±1.0*	8.9 *±7.8*	13.9 *±2.9*	70.8 *±8.5*	5.1 *±1.9*
Z4	70.1 *±18.4*	11.5 *±6.8*	16.6 *±12.1*	0.2 *±0.1*	11.8 *±8.9*	16.6 *±3.1*	69.2 *±9.9*	2.4 *±1.0*	11.8 *±9.3*	12.7 *±2.3*	71.5 *±8.9*	3.6 *±1.8*
Z5	74.6 *±12.3*	12.3 *±6.2*	12.4 *±6.3*	0.3 *±0.1*	13.7 *±7.9*	16.0 *±2.3*	65.3 *±6.9*	4.0 *±0.8*	12.4 *±8.4*	15.7 *±3.9*	64.8 *±6.4*	6.9 *±2.5*
Z6	80.1 *±11.2*	9.4 *±4.9*	10.5 *±6.8*	0.3 *±0.2*	16.1 *±6.8*	17.7 *±3.7*	61.9 *±7.2*	3.7 *±1.0*	17.0 *±7.7*	13.8 *±3.3*	64.8 *±7.3*	5.2 *±1.8*
Z7	81.0 *±2.1*	8.4 *±1.8*	9.0 *±1.5*	1.3 *±0.3*	22.6 *±3.4*	12.2 *±2.4*	51.5 *±2.5*	13.2 *±2.6*	15.1 *±2.2*	10.1 *±2.0*	63.6 *±2.4*	10.9 *±1.4*

Table 4. NPP production per ultraphytoplankton group (mg C m^{-3} d^{-1}) (min, max and mean under brackets) values calculated using Equation (3) by zone.

Group	***Z1***	***Z2***	***Z3***	***Z4***	***Z5***	***Z6***	***Z7***
Synechoccocus	1.3-12.0 (4.8)	13.9-23.1 (18.5)	0.8-4.8 (2.2)	0.3-4.1 (1.6)	0.4-2.6 (1.2)	0.7-4.2 (5.2)	0.9-9.4 (3.0)
Picoeukaryotes	0.6-5.2 (2.4)	2.6-3.1 (2.8)	1.1-2.4 (1.6)	0.4-3.3 (1.7)	0.4-1.2 (0.8)	0.6-7.9 (1.3)	0.5-2.1 (2.7)
Nanoeukaryotes	0.7-14.6 (5.3)	8.1-14.9 (11.5)	1.9-6.2 (3.4)	0.7-3.3 (1.7)	0.5-0.7 (0.7)	1.6-5.0 (4.0)	0.9-7.1 (2.6)
Cryptophytes-like	1.0-12.5 (3.3)	3.1-4.4 (3.8)	0.7-4.1 (1.7)	0.3-1.8 (0.8)	0.2-0.9 (0.6)	0.3-4.6 (1.2)	0.6-1.7 (1.9)

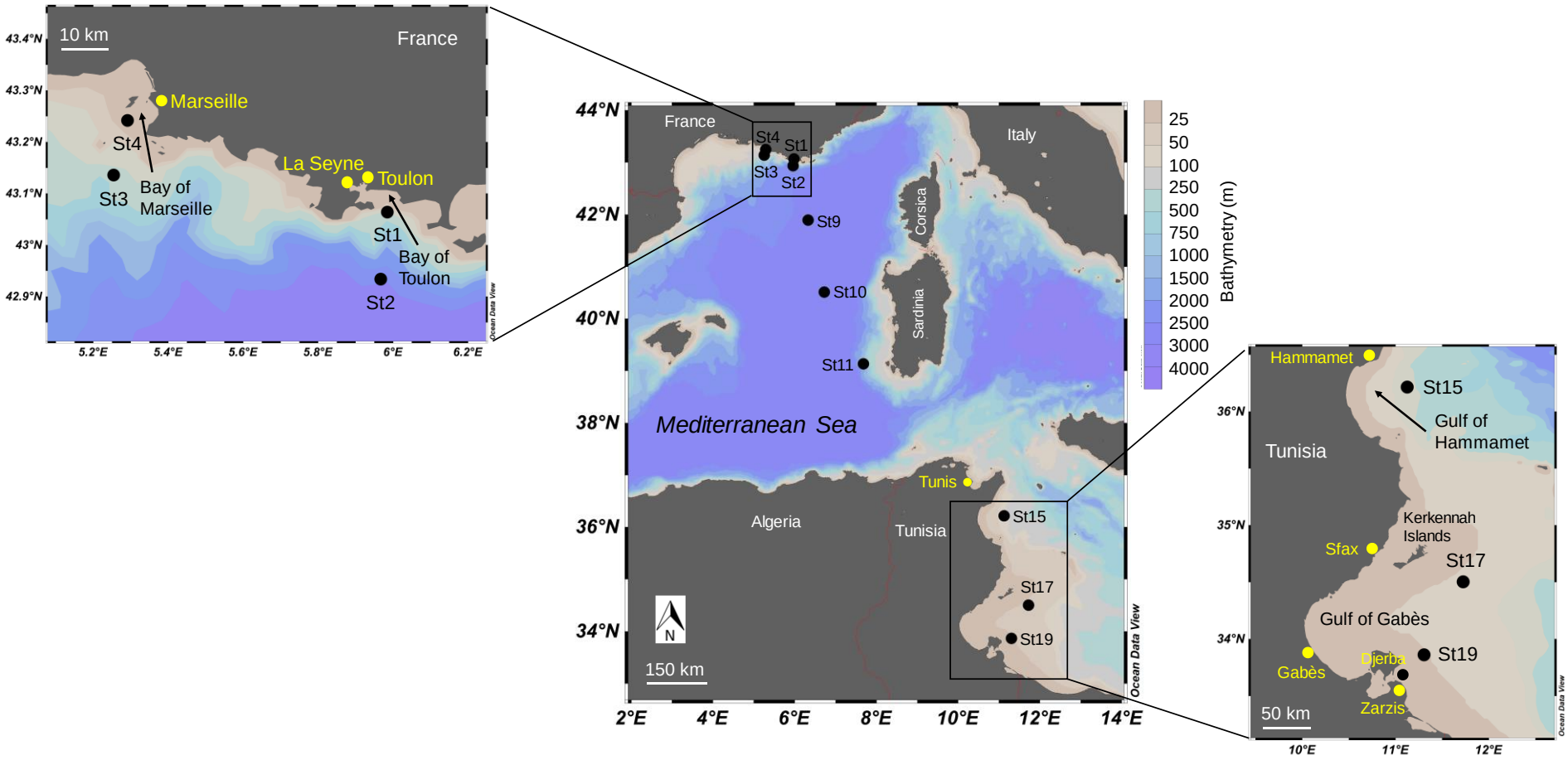

Figure 1 Map of the MERITE-HIPPOCAMPE cruise track in the Mediterranean Sea with the positions of the ten stations sampled.

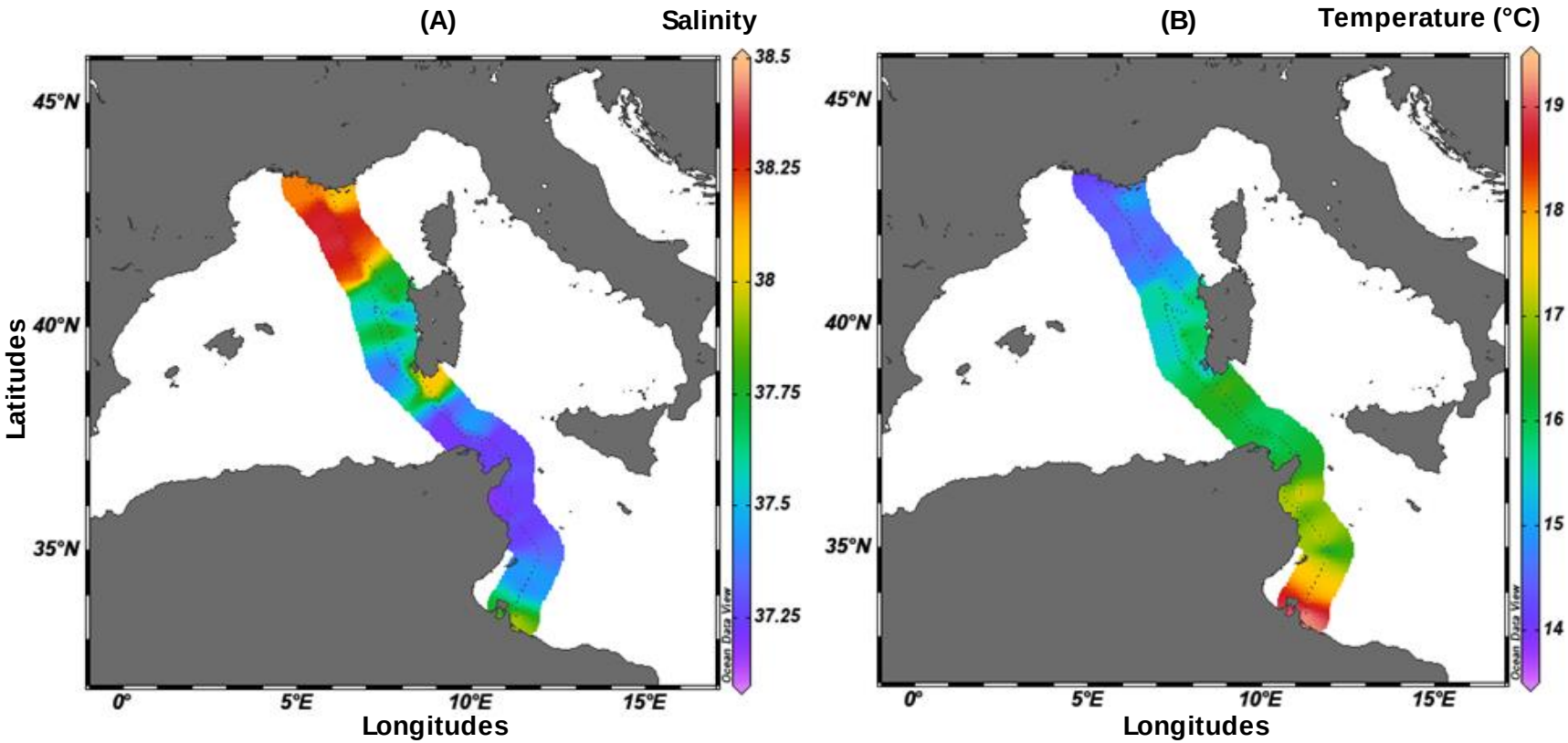

Figure 2 Subsurface temperature (A) and salinity (B) distributions along the Mediterranean transect during the MERITE-HIPPOCAMPE cruise

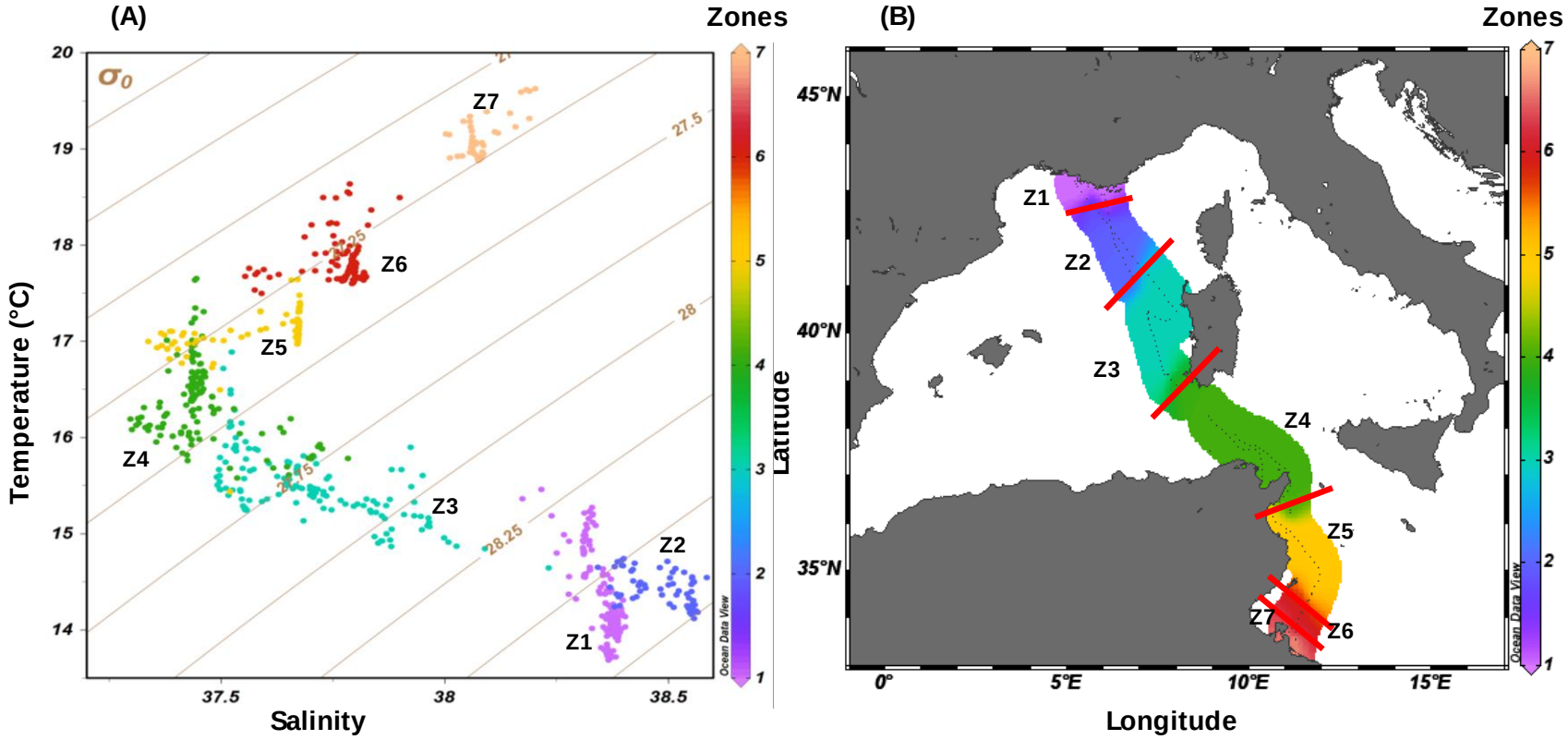

Figure 3 Temperature vs salinity of subsurface waters (A) sampled at 2-m depth. Surface distribution of the 7 zones along the round trip transect (B).

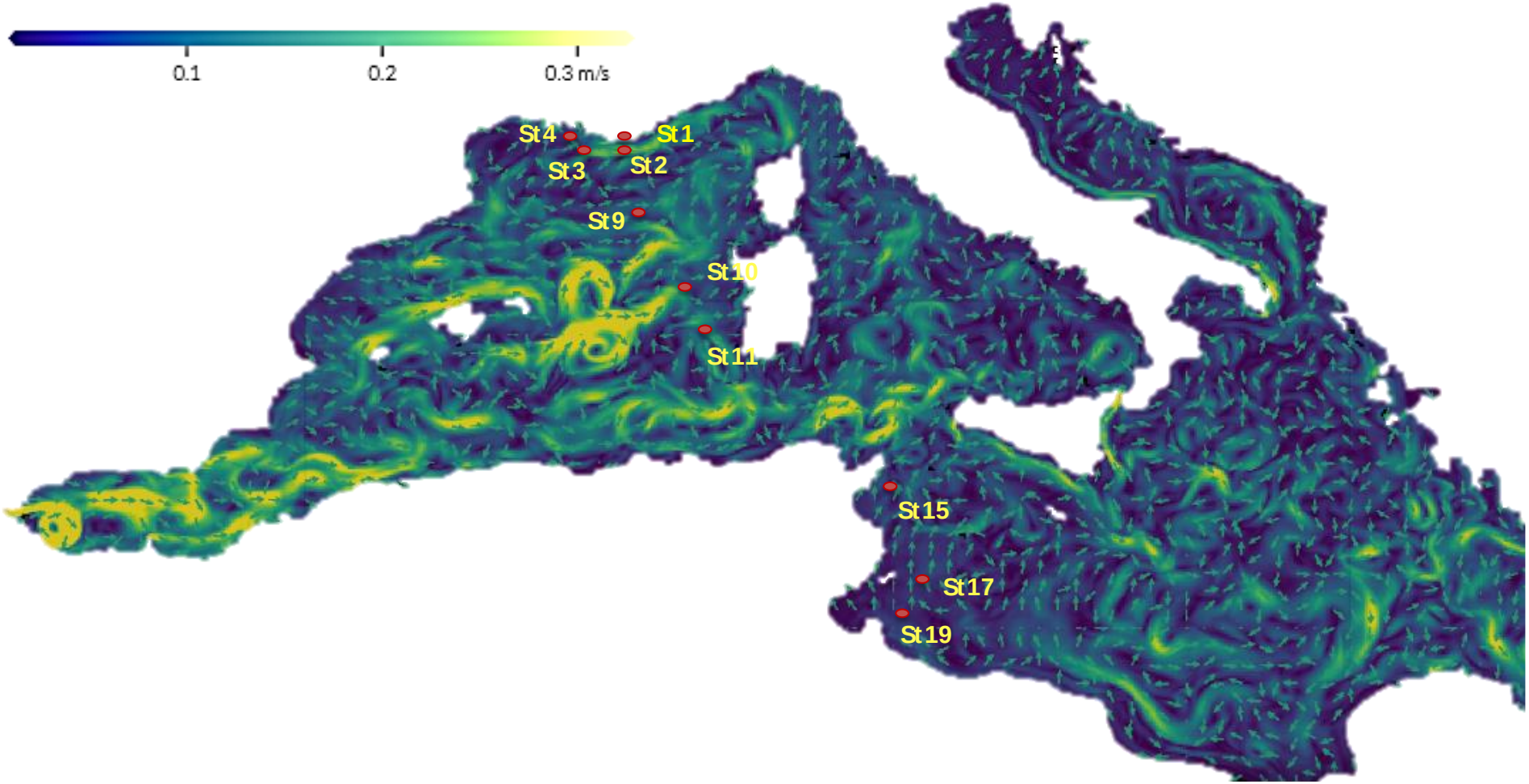

Figure 4 Surface water velocity map of the Mediterranean Sea on May 8th, 2019 (from MyOcean Pro COPERNICUS online interface)

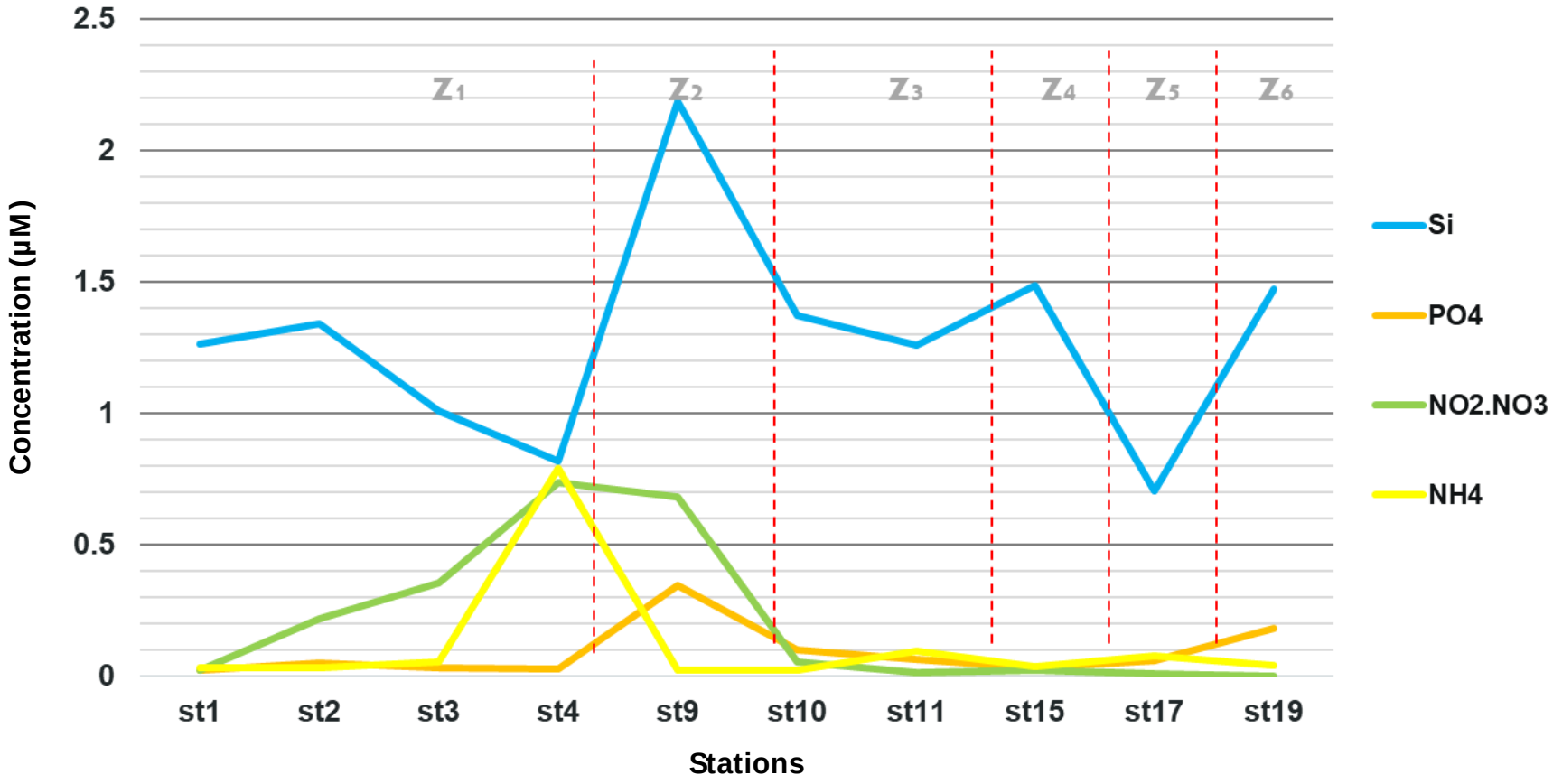

Figure 5 Concentrations (µM) of $Si(OH)_4$ (blue line), PO_4^{3-} (orange line), $NO_3^- + NO_2^-$ (green line) and NH_4^+ (yellow line) in subsurface waters (5-m depth) at the ten stations. Zone 7, which does not contain any of the ten stations (and thus no nutrient data), is not displayed here.

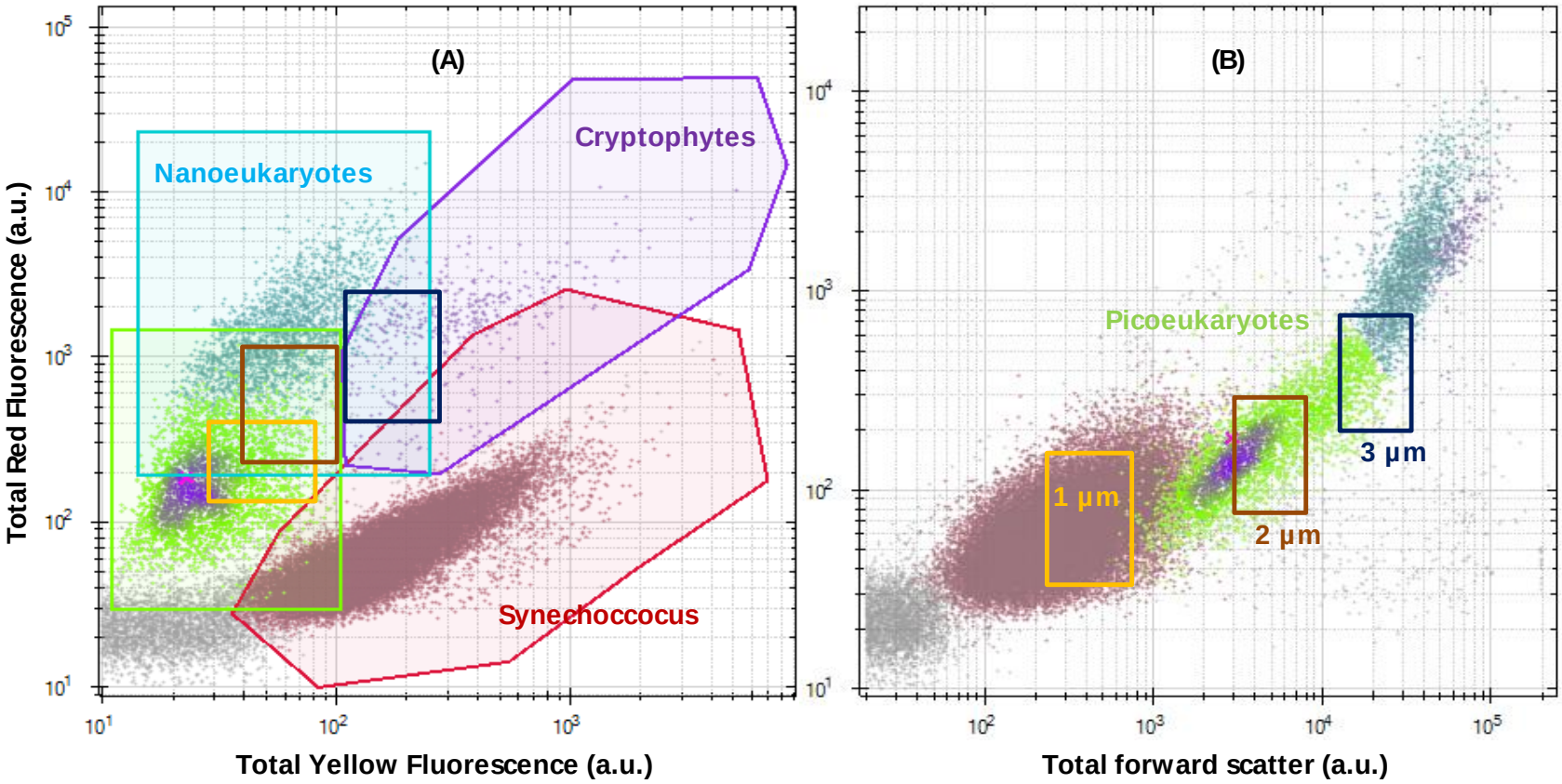

Figure 6. Cytograms representing the Total Red Fluorescence (Total stands for area under the pulse shape curve, a.u.) vs Total Yellow Fluorescence (a.u.) signatures used to classify Synechococcus and Cryptophytes-like (A) and the Total Red fluorescence (a.u.) vs the Total Forward scatter (a.u.) for the classification of picoeukaryotes and nanoeukaryotes (B). Scares represent the areas where silica beads are observed as a memory footprint for size classification.

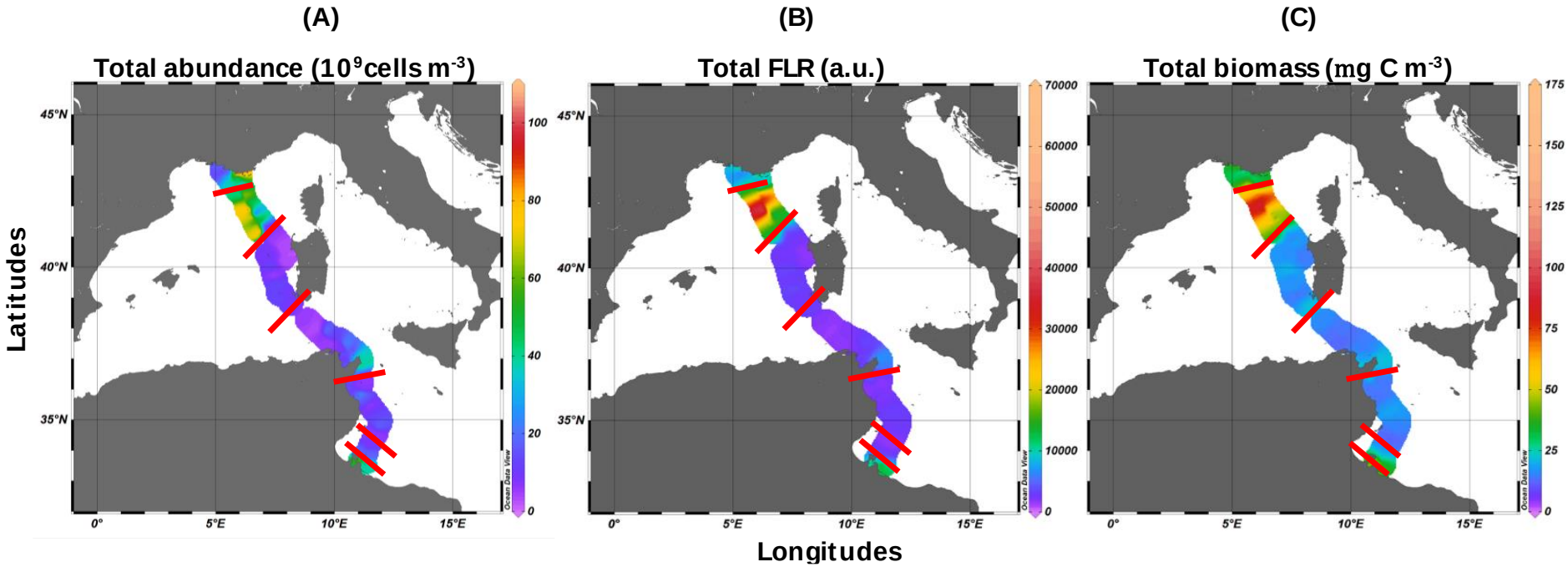

Figure 7. Distribution of total (sum of each ultraphytoplankton group) abundance (10^{-3} cells m^{-3}) (A), FLR per unit of volume (a.u. m^{-3}) (B), and biomass (mg C m^{-3}) (C) in the subsurface waters of the round trip transect.

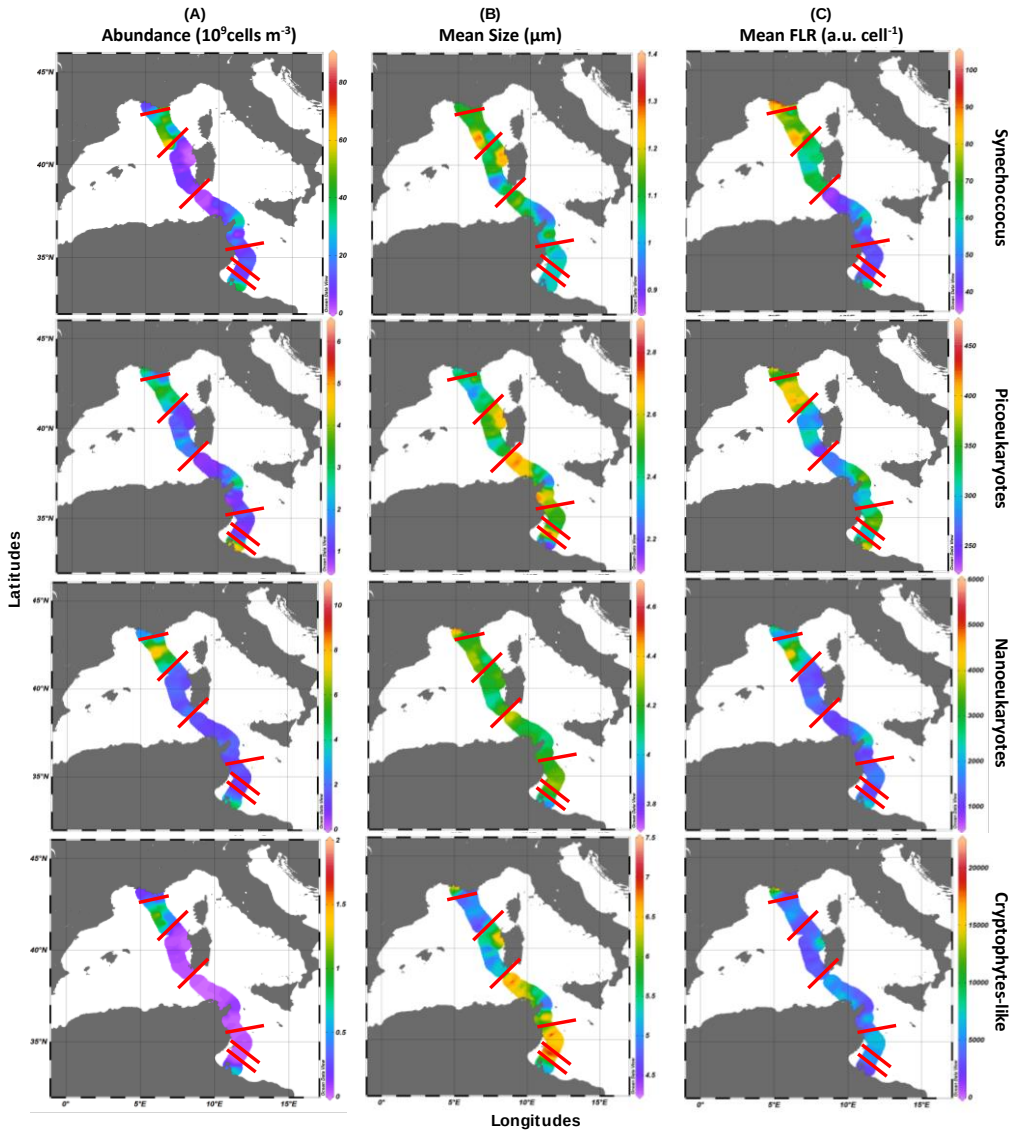

Figure 8 Spatial distribution of the abundances (10^9 cells m^{-3}) (A), mean cell size (µm) (B) and mean FLR (a.u. $cell^{-1}$) for the four resolved groups. Red lines represents the 7 zones (Z1 to Z7) generated by hierarchical classification.

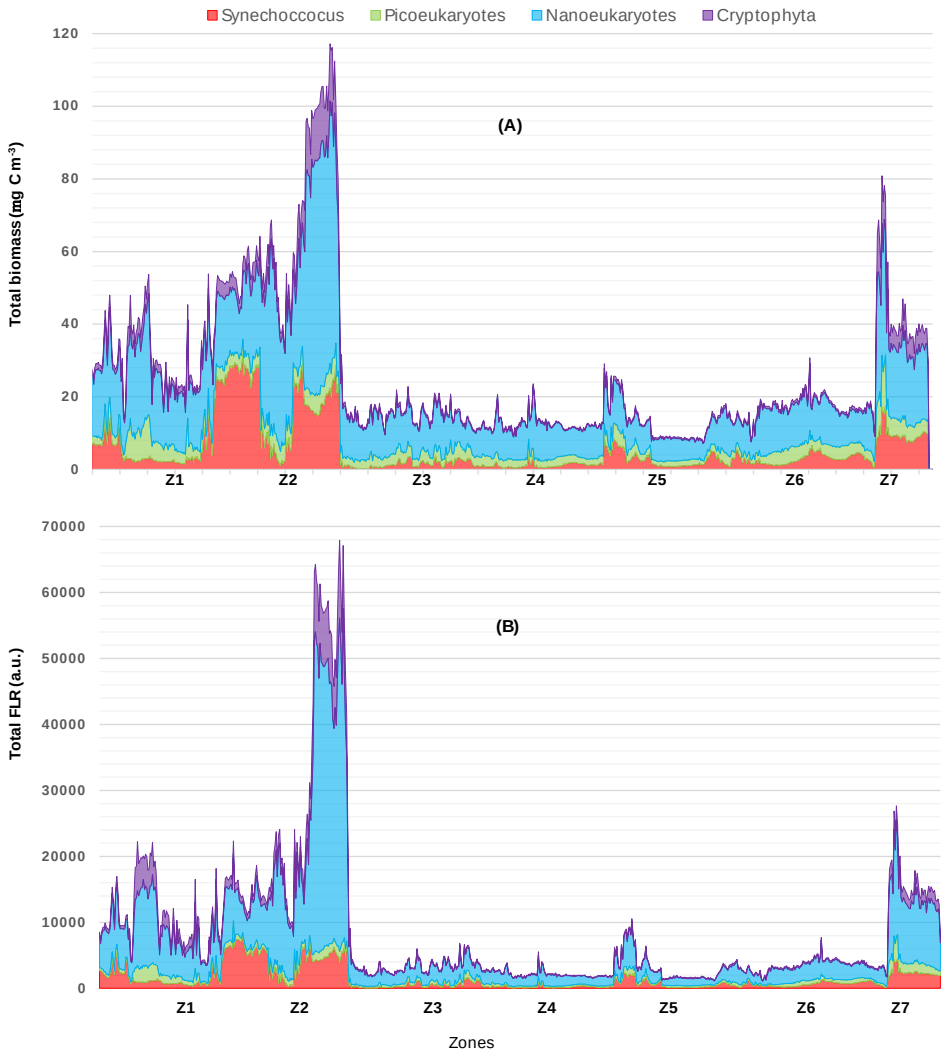

Figure 9 Total biomass contribution of Synechoccocus, picoeukaryotes, nanoeukaryotes and Cryptophytes-like along the 7 zones in terms of biomass (mg C m^{-3}) (A) and FLR_{cell} (B)

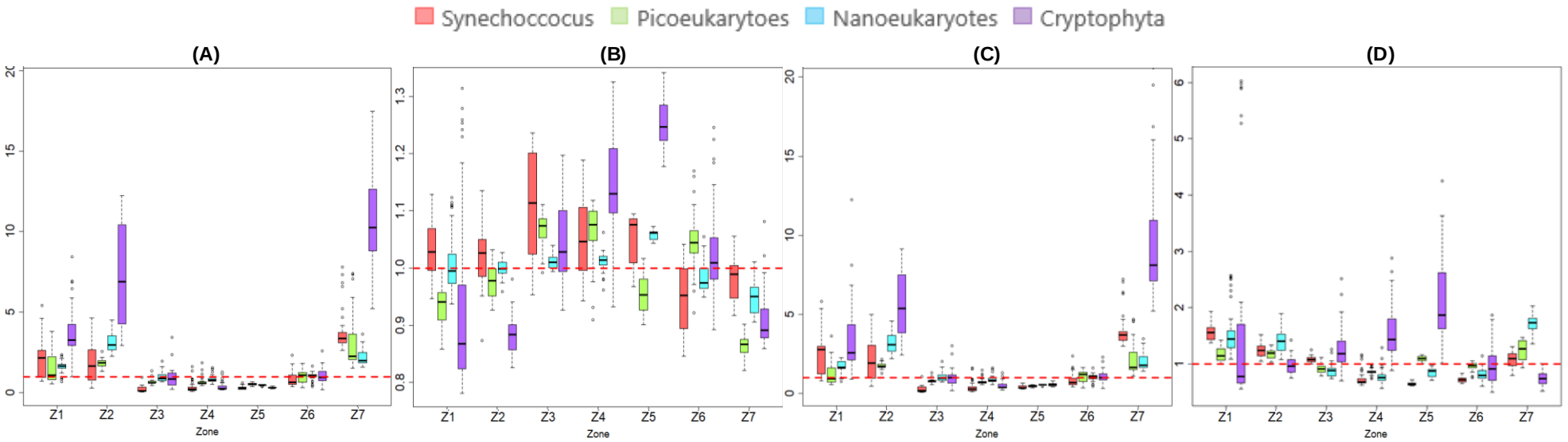

Figure 10 Spatial variability of median-normalized abundance (A), mean size (B), FLR_{cell} (C) and biomass (D) for each ultraphytoplankton group; with red line representing the normalized median =1

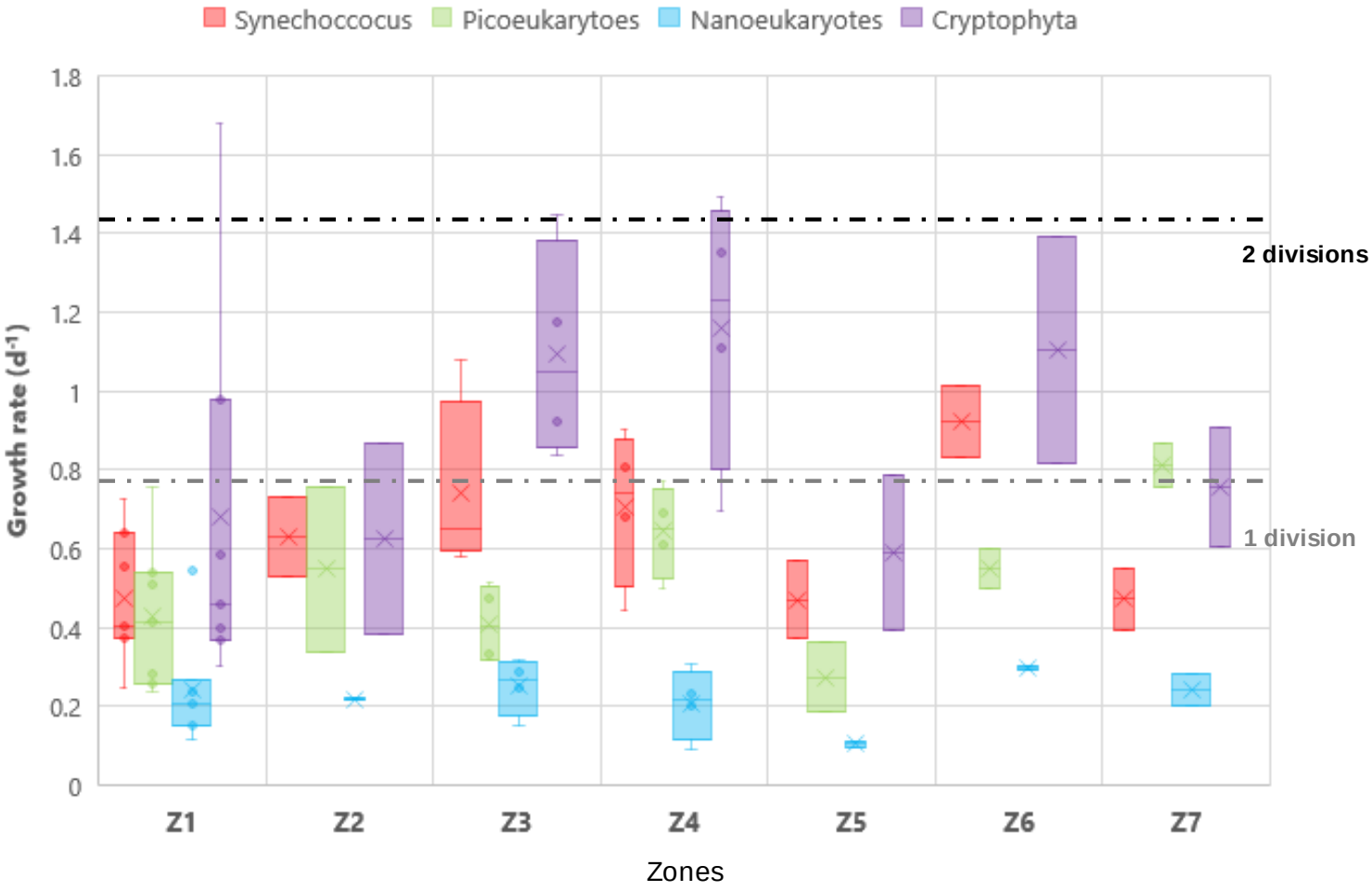

Figure 11 Growth rate variation by zones for the Synechoccocus, picoeukaryotes, nanoeukaryotes and Cryptophytes-like with 0.69 (grey dotted line) and 1.38 (black dotted line) respectively corresponding to 1 and 2 divisions per day